Pergamon

Planet. Space Sci., Vol. 43, No. 12, pp. 1485–1516, 1995

0032-0633/95 $9.50+0.00

0032-0633(95)00064-X

Detectability of molecular species in planetary and satellite atmospheres from their rotational transitions

Th. Encrenaz,[1] B. Bézard,[1] J. Crovisier,[1] A. Coustenis,[1] E. Lellouch,[1] S. Gulkis[2] and S. K. Atreya[3]

[1] Observatoire de Paris, F-92195 Meudon, France
[2] Jet Propulsion Laboratory, California Institute of Technology, Pasadena, CA 91109, U.S.A.
[3] The University of Michigan, Ann Arbor, MI 48109-2143, U.S.A.

Received 26 June 1994; revised 28 March 1995; accepted 29 March 1995

Abstract. High-resolution spectroscopy in the millimeter and submillimeter range has made significant contributions to the study of chemical composition and thermal structure of planetary and satellite atmospheres. This field of research is expected to make considerable progress in the future, from both ground-based and space experiments, with the availability of heterodyne receivers at frequencies up to 1 THz, and with the development of space missions devoted to the exploration of the far-infrared and submillimeter range. A compilation of guidelines for searching molecular species in planetary atmospheres through their rotational transitions, from the millimeter to the far-infrared range (100 μm) is presented. These transitions are specified, and the corresponding synthetic spectra are shown, or detectability limits are estimated. Several observational scenarios are considered: (1) ground-based heterodyne observations (such as those with IRAM, CSO, JCMT); (2) space heterodyne observations with a 3 m antenna (such as that on the European FIRST space mission); (3) Fabry–Pérot spectroscopic observations from the ground and from space (such as the ISO and FIRST space missions). All planets (except Mercury) and the three satellites surrounded by an atmosphere, Titan, Triton and Io, are considered. The main results of this compilation can be summarized as follows. In addition to previously detected molecules, several species appear as promising candidates for detection in the far-infrared to millimeter spectral range. For ground-based heterodyne observations, they include: HCl, O_3 and SO on Venus; HCl, O_3, H_2O_2 and NO on Mars; HCl in the giant planets; SO on Io. For space observations, they are: O_2 on Venus and Mars (provided Venus is observable with FIRST), H_2O in Saturn and Titan (with ISO and FIRST); HD, HCl and other halides in the giant planets (ISO). In the case of heterodyne observations, detectability limits are also indicated. They typically correspond to mixing ratios in the range 10^{-8}–10^{-10}, depending upon the strength of the observed transition. It should be noted that a 30 m antenna operating at 230 GHz remains very competitive, especially for small objects (e.g. Io) with large dilution factors. Heterodyne observations of Triton and Pluto appear beyond the limit of detection.

1. Introduction

The study of planetary atmospheres provides important clues for understanding the origin, evolution, and more generally the formation processes of the terrestrial and giant planets. Planetary atmospheres undergo continuous processing and change throughout their lifetimes. Both transport (diffusion, convection, escape, and winds) and physico-chemical effects (photochemistry, electrochemistry, and thermochemistry) act to change the state of planetary atmospheres. Volcanism and strong convection may suddenly induce disequilibrium processes, leading to the presence of unexpected atmospheric components. A thorough understanding of these complex processes is required for understanding the history of planetary atmospheres. Significant progress in this area can be made by detecting, measuring and analyzing trace atmospheric constituents, including their horizontal and vertical distributions, and their temporal and spatial variations.

Heterodyne spectroscopy in the millimeter and submillimeter range is especially suited for the study of atmospheric processes. The heterodyne technique gives access to very high spectral resolution. Resolving powers of 10^6 and higher with bandwidths of 0.5–1 GHz are presently

Correspondence to: Th. Encrenaz

Table 1. Molecular radio lines detected in planets and satellites

Frequency (MHz)	Species	Transition	Planet(s)[a] V	M	J	S	U	N	P	I	T	SL-9/J
22235	H_2O	6_{16}–5_{23}		*								?
23694	NH_3	(1, 1)–(1, 1)			*	*(from broad band abs.)						
89088	HCN	1–0						*			*	*
115271	CO	1–0	*	*				*			*	*
143057	SO_2	16, 2, 14–16, 1, 15								*		
145561	HC_3N	16–15									*	
146605	SO_2	4, 2, 2–4, 1, 3								?		
1471XX	CH_3CN	(8, K)–(7, K)[b]									*	
183310	H_2O	3_{13}–2_{20}	*	?								
214689	SO_2	16, 3, 13–16, 2, 14								*		
216643	SO_2	22, 2, 20–22, 1, 21								*		
218325	HC_3N	24–23									*	
218903	OCS	18–17										*
219560	$C^{18}O$	2 1	*									
219949	SO	6(5)–5(4)								?		
220399	^{13}CO	2–1	*	*							*	
2207XX	CH_3CN	(12, K)–(11, K)[b]									*	
221965	SO_2	11, 1, 11–10, 0, 10								*		
225897	HDO	3_{12}–2_{21}	*	?								
230538	CO	2–1	*	*				*				*
244936	CS	5–4										*
258157	$HC^{15}N$	3–2									*	
259012	$H^{13}CN$	3–2									*	
265886	HCN	3–2						*			*	*
266944	PH_3	(1, 0)–(0, 0)				*						
345795	CO	3–2						*				
346652	SO_2	19, 1, 19–18, 0, 18								?		
354505	HCN	4–3						*			*	*
461041	CO	4–3									*	

[a] V, Venus; M, Mars; J, Jupiter; S, Saturn; U, Uranus; N, Neptune; P, Pluto; I, Io; T, Titan; SL-9/J, impact of comet Shoemaker–Levy-9 on Jupiter.
[b] Several transitions are observed near the same frequency; the last digits of the frequency are not given.

achievable. This very high resolving power allows the retrieval of the vertical distribution of the observed molecule and/or of the atmospheric thermal profile. In addition, this technique allows the detection of molecules with very low mixing ratios, due to the strong intensity of many rotational transitions, and the large size of ground-based antennas. After the early detections of CO on Mars and Venus (Kakar *et al.*, 1976, 1977), many attempts have been made to detect and/or monitor rotational transitions in the atmospheres of planets and satellites, leading to several significant discoveries. Among the most remarkable results of the past few years, one should note the first detections of CO and HCN on Neptune (Marten *et al.*, 1991, 1993), HC_3N and CH_3CN on Titan (Bézard *et al.*, 1992, 1993a), SO_2 on Io (Lellouch *et al.*, 1990), HDO and H_2O on Venus and possibly Mars (Encrenaz *et al.*, 1991a,b, 1995a,b). Vertical distributions of CO (Muhleman *et al.*, 1984; Marten *et al.*, 1988) and HCN (Tanguy *et al.*, 1990) on Titan were retrieved. In the atmospheres of Venus and Mars, the CO abundance and thermal structure were monitored over long-time periods (Clancy and Muhleman, 1985). Finally, heterodyne millimeter CO measurements have been used to measure wind velocities in the atmospheres of Mars and Venus (Lellouch *et al.*, 1991b; Pierce *et al.*, 1991). Table 1 gives the list of molecular radio lines detected in planetary and satellite atmospheres.

The unexpected detection of stratospheric CO and HCN in Neptune, but not in Uranus, provides a good example of the importance of detecting minor constituents in planetary atmospheres. These constituents were detected in the submillimeter range with mixing ratios of about 1 ppb and 1 ppm for HCN and CO, respectively (Marten *et al.*, 1991, 1993). Subsequent observations performed in the millimeter range (Rosenqvist *et al.*, 1992) yield a factor of 4 lower mole fraction for HCN and a factor of 2 lower mole fraction for CO. A satisfactory explanation of this discrepancy could be important in constructing models of the origin of these constituents. CO is believed to be of internal origin, but present thermochemical models do not account for the observed abundance. HCN is likely to form in the stratosphere by photochemistry involving nitrogen atoms; these could originate either from Neptune's satellite Triton, or from the dissociation of molecular N_2 (coming from Neptune's interior) by galactic cosmic rays. In the latter case, the existence of CO and N_2 in this planet would give an important insight into the origin of the giant planets' atmospheres, by constraining models of the chemical composition of the primordial solar nebula. The above

example shows that minor constituents can provide important clues to the formation of the planets. Clearly, improved measurements will be needed to better constrain the models.

The collision of comet Shoemaker–Levy-9 with Jupiter, in July 1994, provided another opportunity for monitoring the Jovian stratosphere using heterodyne spectroscopy. Through their millimeter and submillimeter transitions, several new species (CO, CS, OCS, HCN) were detected in the Jovian stratosphere, as a result of shock chemistry following the explosion of the fragments (Lellouch *et al.*, 1995; Marten *et al.*, 1995). In addition, the monitoring of these lines provided a direct measurement of the stratospheric temperature above the 1 mbar pressure level: the observed lines first appeared in emission, then turned into absorption lines one week after the impacts, and remained observable for several months. This shows evidence for a persistent cooling of the Jovian stratosphere, possibly due to the formation of stratospheric haze.

Over the past decade, technological developments have been achieved in two specific directions which lead us to foresee a significant advancement in this field of research in the years to come: the extension of sensitive heterodyne receivers to higher frequencies, and the capability of operating large submillimeter telescopes in space above the Earth's atmosphere.

Sensitive heterodyne receivers using SIS mixers, are currently available at frequencies up to 700 GHz; it is expected that the frequency range will extend to 1 THz and possibly higher by the end of this decade. The use of higher frequencies will be essential for two reasons. First, present observations are currently limited by the diffraction limit of the telescope. Even a 30 m antenna has a diffraction limit of 12 arcsec at 230 GHz, which strongly restrains the imaging capabilities of these observations. This difficulty can be overcome either by the use of millimeter interferometers, or by the extension toward higher frequencies. The second advantage lies in the larger choice of available transitions, allowing new molecules to be searched for, and stronger transitions to be used, implying improved detectability limits.

At the same time, space missions are now under development for the exploration of the infrared and submillimeter spectral range. The ISO mission (Infrared Space Observatory), to be launched by ESA in 1995, will explore the infrared sky up to a wavelength of 180 μm. There is no heterodyne spectroscopy on board, but a Fabry–Pérot, which is of interest for the present study. As a next step, the FIRST mission (Far Infrared Space Telescope), also to be launched by ESA around 2006, will be instrumented with low noise heterodyne receivers for a full spectral coverage by heterodyne spectroscopy up to a frequency of about 1 THz, and by Fabry–Pérot spectrometers at higher frequencies. In addition, in the specific case of Saturn and Titan, the Cassini mission, to be launched by NASA and ESA in 1997, will carry on its orbiter a far-infrared interferometer spectrometer (CIRS). In spite of its much lower spectral resolving power, as compared with the previous above-mentioned capabilities, this instrument will offer interesting opportunities due to its high spatial resolution. All these space missions will enlarge

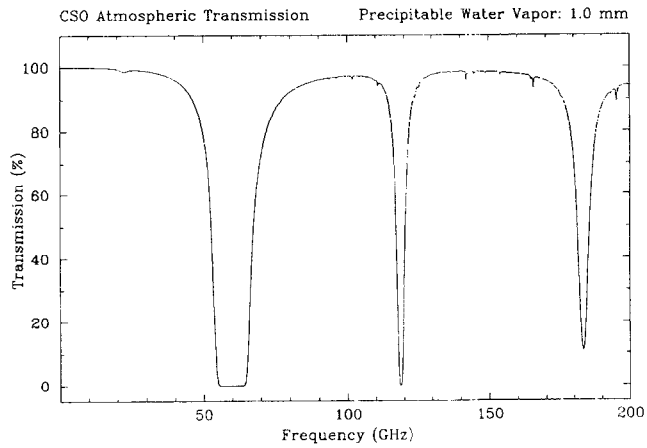

Fig. 1. Synthetic spectrum of the atmospheric transmission calculated for 1 mm-ppt water vapor. This corresponds to typical conditions at Mauna Kea (altitude 4 km). Spectral range: 0–200 GHz

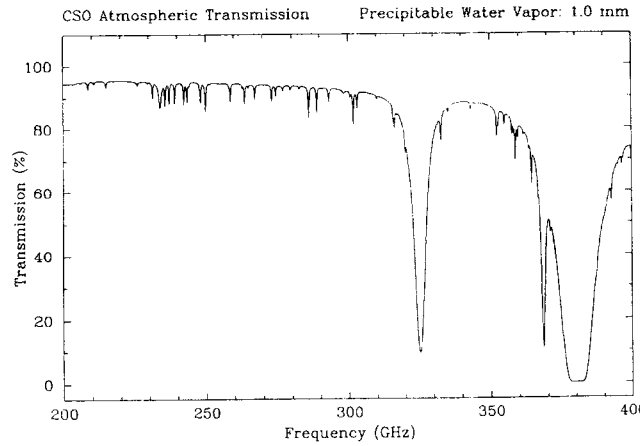

Fig. 2. Same as Fig. 1. Spectral range: 200–400 GHz

the observable spectral range to regions obscured by the terrestrial opacity, allowing, in particular, the observation of molecules like H_2O and O_2, but also NH_3 and many other species. Figures 1–5 show the atmospheric opacity from the far-infrared to the millimeter range (corresponding to frequencies lower than 1 THz), at a high-altitude observatory (Mauna Kea, Hawaii).

In order to take full advantage of these new oppor-

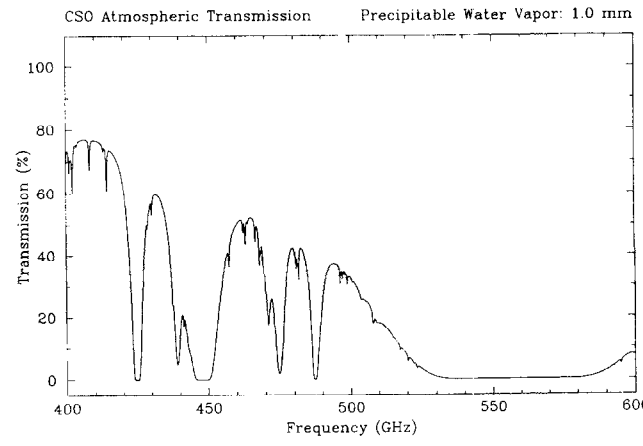

Fig. 3. Same as Fig. 1. Spectral range: 400–600 GHz

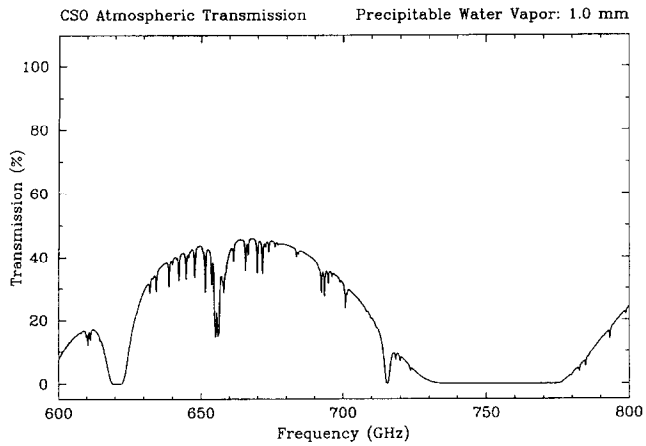

Fig. 4. Same as Fig. 1. Spectral range: 600–800 GHz

tunities, it is necessary to make a systematic study of the transitions available for each species which might be present in a planetary atmosphere, and to estimate the corresponding detectability limits. The objective of this paper is to make such a compilation, by taking a list of possible molecules, defining the best spectral range for their detection, and calculating for each planet the corresponding detectability limit for a given type of observation. The aim of this study is to help in the definition of future planetary observations in the far-infrared, submillimeter and millimeter range, from the ground and from space. A preliminary version of this analysis can be found in Encrenaz *et al.* (1991c).

The basic principles of line formation in planetary atmospheres at thermal wavelengths are discussed in Section 2. Various types of possible observations, from the ground and from space are presented in Section 3. The selection of molecules to be considered is discussed in Section 4, and the model used is presented in Section 5. Our results, listed by object, are given in Section 6, and our conclusions are summarized in Section 7.

2. Line formation in planetary atmospheres

We consider the case of a planetary or a satellite atmosphere in which the lines are Lorentz-broadened (Townes and Schawlow, 1955; Hanel *et al.*, 1992; Janssen, 1993).

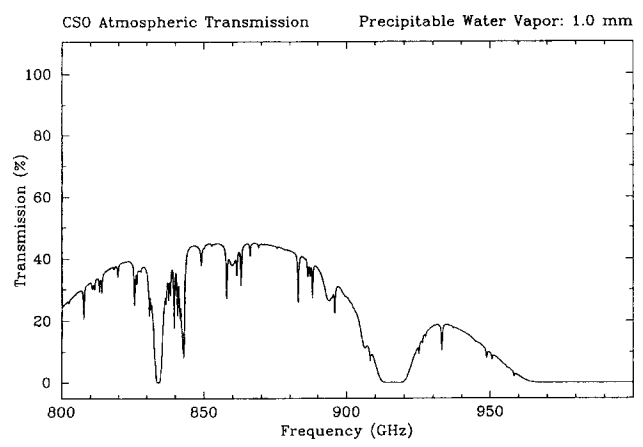

Fig. 5. Same as Fig. 1. Spectral range: 800–1000 GHz

This is a valid assumption in most cases, with the exception of very tenuous atmospheres (Io, Triton, Pluto) and the upper stratospheres, when pressures are lower than about 100 μbar. At infinite spectral resolution, the absorption coefficient at the line center, in cm^{-1}, is defined as

$$\alpha(cm^{-1}) = \frac{S}{\pi} \cdot \frac{N}{\Delta\nu} \tag{1}$$

where S is the line strength, in cm per molecule, N the number of molecules per cm^3, and $\Delta\nu$ the half-width of the line at half-maximum, in cm^{-1} (we note that α, through S, is temperature dependent).

The number density of molecules N of a specific minor constituent is given by

$$N = \frac{\rho P}{kT} \tag{2}$$

where P is the total pressure, T the temperature, and ρ the mixing ratio, per volume, of the minor constituent (assumed to be constant); k the Boltzmann constant.

The half-width of the line $\Delta\nu$ is well represented by the following formula (Townes and Schawlow, 1955):

$$\Delta\nu = \gamma_0 P \left[\frac{300}{T}\right]^X \tag{3}$$

where γ_0 is the broadening coefficient, in $cm^{-1}\ atm^{-1}$, measured at a temperature of 300 K. X is a coefficient varying from about 0.5 to 1, depending upon the interaction potential between the minor constituent and the main atmospheric gas responsible for the line broadening. We thus derive

$$\alpha = \frac{S\rho}{\pi\gamma_0 k T^{1-X} 300^X}. \tag{4}$$

We will now derive the minimum detectable mixing ratio of a minor constituent as a function of the line strength. The theory of radiative transfer in a planetary atmosphere can be found in Goody (1964) or Hanel *et al.* (1992). In the case of an object with a surface, under normal incidence, we have

$$I_\nu = \varepsilon_0 B_\nu(T_s)\, e^{-\tau_0} + \int_0^{\tau_0} B_\nu(T)\, e^{-\tau(z)}\, d\tau(z) \tag{5}$$

where I_ν is the outgoing intensity at the line center, B_ν the Planck function, T_s the surface temperature, and ε_0 the surface emissivity. τ_0 is the total optical depth of the atmosphere (from surface to free space), τ the optical depth above the level of altitude z:

$$\tau(z) = \int_z^\infty \alpha(z')\, dz'. \tag{6}$$

Except in the case of the coldest objects ($T < 100$ K) in the high-frequency range of the submillimeter region ($\nu > 600$ GHz), the brightness integral can be written using the Rayleigh–Jeans approximation of Planck's law:

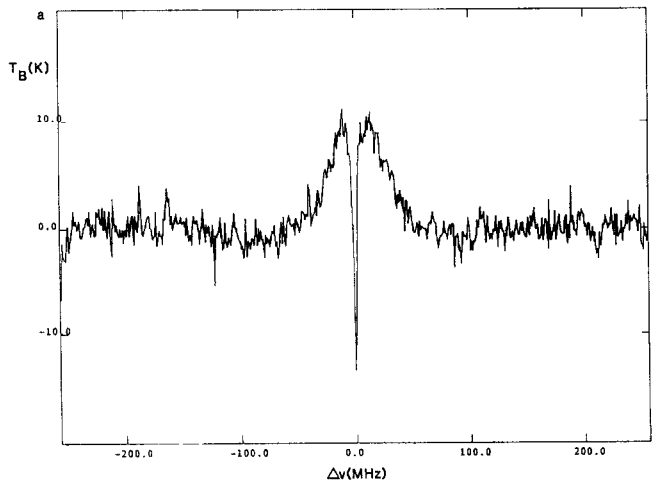

Fig. 6. Observed spectrum of the CO ($J = 1$–0) transition on Mars, at 115 GHz. The figure is taken from Lellouch *et al.* (1989). The continuum level has been removed

$$T_c = \varepsilon_0 T_s e^{-\tau_0} + \int_0^{\tau_0} T(z)\, e^{-\tau(z)}\, d\tau(z) \qquad (7)$$

where T_c is the brightness temperature at the line center.

In particular, assuming a constant atmospheric temperature T_a above the surface, equation (7) can be rewritten as follows:

$$T_c = \varepsilon_0 T_s e^{-\tau_0} + T_a(1 - e^{-\tau_0}). \qquad (8)$$

In the case of a weak, optically thin line ($\tau_0 \ll 1$), this equation becomes

$$T_c - \varepsilon_0 T_s = \Delta T \sim (T_a - \varepsilon_0 T_s)\tau_0. \qquad (9)$$

Equation (9) shows that the temperature contrast between the line center T_c and the continuum ($\varepsilon_0 T_s$), ΔT, is a function of ε_0, τ, and T_a. [In the more general case, the temperature contrast depends on ε_0, τ, and $T(z)$.] We have seen (equation (4)) that the absorption coefficient is directly proportional to $S \cdot \rho$. This illustrates that the line contrast ΔT is proportional to the mixing ratio and the line strength of the line. The broadening coefficient γ_0 is approximately constant, within a factor of about 2, for most of the considered molecules, with a typical value of 0.1 cm^{-1} atm^{-1}, or 3 GHz atm^{-1}. As a consequence, for a given planetary atmosphere, the minimum detectable mixing ratio of a minor constituent is, at first approximation and within an uncertainty of a factor of 2, inversely proportional to the intensity of the transition used for the detection.

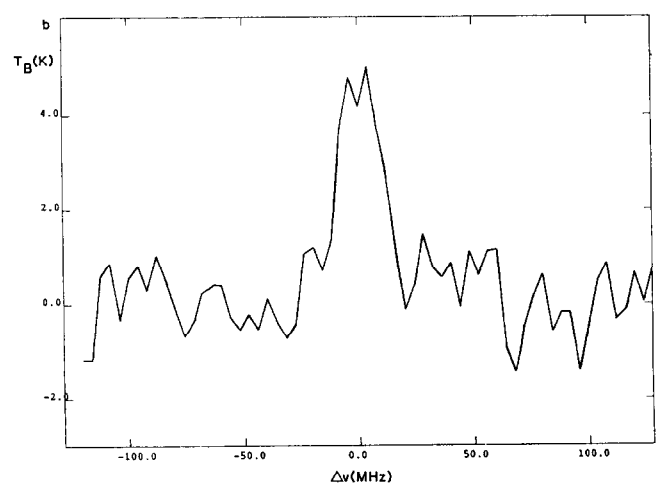

Fig. 7. Observed spectrum of the ^{13}CO ($J = 1$–0) transition on Mars, at 110 GHz. The figure is taken from Lellouch *et al.* (1989). The continuum level has been removed. The temperature contrast due to the limb emission is about 3 K

The minimum detectable temperature difference can be estimated and compared with the line contrast to determine the minimum detectable mixing ratio for a specific molecule. In the case of a source filling the field of view, the minimum detectable temperature difference is a function of the system temperature T_{sys}, the bandwidth B and the integration time t. If the source does not fill the field of view, the minimum detectable temperature is calculated using the factors above and the beam filling factor. The system temperature depends upon the quality of the receiver and the opacity of the terrestrial atmosphere; the field of view depends on the size of the antenna. These quantities will be calculated in more detail in Section 3.

Figures 6 and 7 show examples of strong and weak lines observed in the atmosphere of Mars. In this case, the atmospheric temperature decreases regularly from the surface temperature T_s down to a constant value T_a at about $z = 50$ km. For an emissivity factor ε_0 of about 0.9, in the case of the CO ($J = 1$–0) transition, the strong line exhibits a continuum temperature of $0.9T_s$, a maximum temperature of T_s in the wing (corresponding to an optical depth of unity just above the surface) and a narrow absorption line in the core, with a temperature close to T_a at the line center (Fig. 6). In the case of the weak ^{13}CO ($J = 1$–0) line, the limb contribution becomes dominant, and the line is seen in emission (Fig. 7).

In the case of dense planetary atmospheres, the continuum outside the line is not due to a surface or a cloud deck, but is defined by a continuous spectral absorption due to the wings of other strong lines (as, for example, NH_3 for Jupiter) and/or the pressure-induced spectrum of the dominant atmospheric constituent (hydrogen for the giant planets, CO_2 for Venus, N_2 for Titan). The thermal profiles of the giant planets show an inversion at the tropopause (P close to 100 mbar), with a negative temperature gradient in the troposphere and an increase of the temperature with altitude above. Strong transitions can show a narrow emission core at the center of a very broad absorption line. This is illustrated in Fig. 8 with the CO ($J = 2$–1) spectrum of Neptune. It is important to notice that, because the FWHM of a Lorentz-broadened line is typically a few GHz per atmosphere, any tropospheric line, formed below the 100 mbar level, has a width comparable to or larger than the receiver bandwidth making it difficult to observe with the heterodyne technique. Thus, in the case of the giant planets, heterodyne spectroscopy is best used to detect atmospheric species which are present in their stratospheres.

3. Selection of observational cases

We consider several cases, on the basis of present and future instrument capabilities and observing media. Two

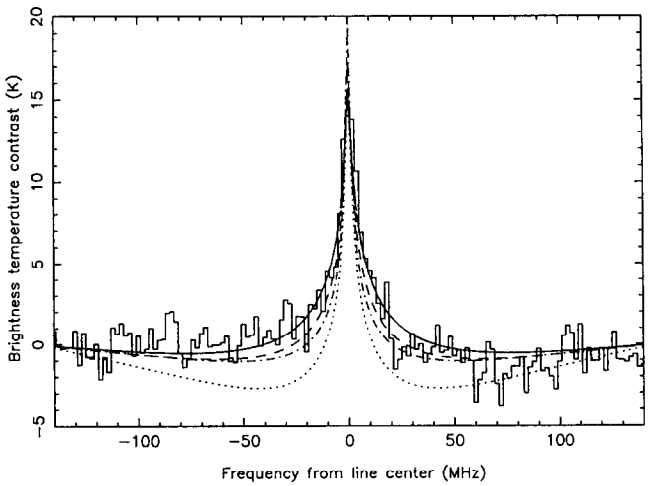

Fig. 8. Observation of the CO (2–1) transition on Neptune, at 230 GHz. The figure is taken from Rosenqvist *et al.* (1992)

types of instrumentation have to be considered. The first one, as described above, is based on coherent detection and provides, through heterodyne spectroscopy, a resolving power of 10^6 over a typical bandwidth of 0.5 GHz; the second one is based on incoherent detection (using, for example, bolometers) and can provide a typical resolving power of about 10^4; the spectral range can be large (several tens of cm^{-1}) if a Fourier-transform spectrometer is used, or much smaller (about 1 cm^{-1}) in the case of a Fabry–Pérot (FP) spectrometer.

Concerning heterodyne spectroscopy, antennas of several tens of meters are presently available, but their efficiency and/or the quality of their site usually limits their frequency range. A typical example is the IRAM (Institut de Radio-Astronomie Millimétrique) 30 m antenna at Pico Veleta (Spain), which is optimized for frequencies lower than 300 GHz. Other antennas of the 10 m class can be used at higher frequencies. Typical examples are the 10.5 m CSO (Caltech Submillimeter Observatory) antenna and the 15 m JCMT (James Clerk Maxwell Telescope) antenna at Mauna Kea Observatory (Hawaii), presently operating at frequencies lower than 700 GHz. With the ongoing development of heterodyne receivers, it can be foreseen that, by the end of this decade, ground-based heterodyne observations with these antennas will be possible up to a frequency of about 1 THz. In the case of incoherent detection, there are a few far-infrared and submillimeter FP spectrometers, which are mostly used on the Kuiper Airborne Observatory; ground-based Fourier-transform spectrometers are also becoming operational.

The opacity of the terrestrial atmosphere strongly limits the spectral range observable from Earth (Figs 1–5). Water vapor and oxygen atmospheric lines prevent astronomical observations in the vicinity of their line centers, making it very difficult to detect these species in astronomical objects, and at the same time preventing the detection of other important molecules such as NH_3, which have transitions falling within the inaccessible spectral ranges. As mentioned above, several space missions involving far-infrared and/or submillimeter instruments are currently under development. In the domain of incoherent detection, the ISO mission, to be launched by ESA in 1995, will explore the infrared sky from Earth orbit during 18 months, providing, in particular, a resolving power of 2×10^4 with a Fabry–Pérot operating in the 45–180 μm range. In the specific case of the exploration of Saturn and Titan, the Cassini mission, to be launched by NASA and ESA in 1997, will carry an infrared interferometer spectrometer (CIRS) providing at best a spectral resolution of 0.5 cm^{-1} in the wavelength range 7 μm–1 mm. Earth-orbit submillimeter space missions have also been considered for exploring the whole submillimeter range with heterodyne spectroscopy. Following the SWASS and ODIN projects, devoted to heterodyne spectroscopy in a few selected channels using 1 m class antennas, the FIRST mission, developed by ESA, is designed for a complete spectral coverage with heterodyne spectroscopy up to a frequency of about 1 THz, using a 3 m antenna. This mission will be completed with incoherent detection Fabry–Pérot instruments operating in the 80–300 μm wavelength range.

On the basis of the achievements and projects described above, we define the following observational cases for our study (Table 2):

(A) Ground-based heterodyne spectroscopy with a 30 m antenna, at frequencies lower than 300 GHz ("IRAM case").

(B) Ground-based heterodyne spectroscopy with a 10 m antenna, at frequencies between 300 GHz and 1 THz ("CSO case").

(C) Heterodyne spectroscopy with a space mission using a 3 m antenna, at frequencies below 1 THz ("FIRST-H case").

(D) Ground-based Fourier-transform spectrometry with a 10 m antenna, at frequencies below 1 THz (wavelengths higher than 300 μm); such an instrument is becoming operational at CSO (Weisstein and Serabyn, 1994).

(E) Fabry–Pérot spectroscopy from space with a 0.60 m telescope, in the wavelength range 100–180 μm (55–100 cm^{-1}; "ISO case").

(F) Fabry–Pérot spectroscopy from space with a 3 m

Table 2. Observational cases

Resolving power	10^6 (heterodyne spectroscopy)	10^4 (Fabry–Pérot/ Fourier-transform spectroscopy)
Ground-based	A (IRAM) $\nu < 300$ GHz $\phi = 30$ m	D (Fourier-transform or FP sub-mm spectrometer)
	B (CSO) 300 GHz $< \nu <$ 1 THz $\phi = 10.5$ m	
Space	C (FIRST-H) $\nu < 1$ THz $\phi = 3$ m	E (ISO) $100 < \lambda < 180$ mu $\phi = 0.60$ m
		F (FIRST-F) $80 < \lambda < 300$ mu $\phi = 3$ m

antenna, in the wavelength range 100 μm–1 mm (frequencies below 100 cm^{-1}, or 3 THz; "FIRST-FP case").

In what follows, we estimate the detectability limits which we can expect for each type of heterodyne experiment (cases A, B and C).

The minimum detectable brightness temperature difference, for a source filling the field of view (FOV), can be estimated as follows:

$$\Delta T_{min} = \frac{K \cdot T_{sys}}{\sqrt{(B \cdot t)}} \quad (10)$$

where T_{sys} is the system temperature in K, B the bandwidth in Hz and t the integration time in s. K is a coefficient approximately equal to 2, the exact number depending on how the receiver is used to observe the planet. The aperture efficiency does not enter the expression if the planet fills the beam. If the source does not fill the FOV, the minimum detectable brightness temperature difference is to be divided by the filling factor. This filling factor depends upon the respective size of the planet and the FOV, and, assuming a gaussian field of view, is defined as follows:

$$f = 1 - 2^{-(\theta/FOV)^2} \quad (11)$$

where θ is the angular diameter of the planet.

We will now calculate the minimum detectable differences of brightness temperatures, for the various planetary and satellite atmospheres, and for the three first cases mentioned above. In all cases we assume $B = 10^6$ Hz (1 MHz spectral resolution) and $t = 3600$ s (1 h integration). The system temperature is a function of both the receiver temperature, which in turn depends upon the frequency, and upon the terrestrial opacity. It also takes into account the telescope efficiency, which tends to degrade as the frequency increases. We include the loss factor of the atmosphere (exp $(-\tau)$) as a divisional term in the calculation of the system temperatures. This substantially increases the system temperature in those spectral regions where the telluric opacity is large. The system temperatures for case B are substantially larger than cases A and C because the atmospheric opacity is large. In case (A), corresponding to IRAM, we adopt a frequency of 230 GHz and $T_{sys} = 600$ K. For cases (B) and (C) (CSO and FIRST-H), we select two values of the frequency: 600 and 900 GHz. At 600 GHz, we take $T_{sys} = 3000$ K for (B) and 300 K for (C); the better performance in (C) is due to the absence of terrestrial opacity. At 900 GHz, we make the following assumption: $T_{sys} = 4500$ K for (B) and 450 K for (C). There numbers are no more than reasonable estimates; actual values can differ by as much as a factor of 2. As an example, IRAM receivers at 230 GHz have presently better system temperatures than indicated in case (A); on the other hand, true values of T_{sys} might be larger than indicated here at high frequencies, if the telescope efficiency is poor.

Table 3 gives the values of the minimum detectable brightness temperature differences, calculated for each object in each of the five cases described above. These results can be interpreted as follows.

(1) A 30 m antenna such as IRAM, operating below 300 GHz, is extremely powerful for all molecules having

Table 3. Detectability limits for cases A, B and C

		Case A (IRAM)		Case B (CSO)		Case B (CSO)		Case C (FIRST)		Case C (FIRST)	
ϕ (m)		30		10.5		10.5		3		3	
ν (GHz)		230		600		900		600		900	
FOV (")		10		12		8		40		27	
T_{sys} (K)		600		3000		4500		300		450	
ΔT_A (K)		0.02		0.10		0.15		0.010		0.015	
Source	(")	f	ΔT_m	f	ΔT_m	f	ΔT_m	f	ΔT_m	f	ΔT_m
Venus	40	1.0	0.02	1.0	0.10	1.0	0.15	0.50	0.02	0.78	0.02
Mars	15	0.79	0.02	0.66	0.15	0.91	0.16	0.093	0.11	0.19	0.08
Jupiter	40	1.0	0.02	1.0	0.10	1.0	0.15	0.50	0.02	0.78	0.02
Saturn	16	0.83	0.02	0.71	0.14	0.94	0.16	0.105	0.10	0.22	0.07
Uranus	3.5	0.08	0.25	0.057	1.7	0.12	1.2	0.0053	1.9	0.011	1.4
Neptune	2.2	0.033	0.60	0.023	4.3	0.051	2.9	0.0021	4.8	0.0046	3.2
Titan	0.8	0.0044	4.5	0.0031	32	0.0069	22	3(−4)	36	6(−4)	25
Io	1.1	0.0083	2.4	0.0058	17	0.013	11	5(−4)	19	0.0011	14
Triton	0.12	1(−4)	200	7(−5)	1440	2(−4)	960	6(−6)	1602	1(−5)	2000
Pluto	0.08	4(−5)	450	3(−5)	3240	7(−5)	2160	3(−6)	3600	6(−6)	2500

Notes:
ϕ (m), antenna or telescope diameter.
ν (GHz), frequency of observation.
FOV ("), field of view.
T_{sys} (K), system temperature.
ΔT_A (K), minimum detectable antenna temperature (r.m.s. for 3600 s integration time at 1 MHz spectral resolution).
f, filling factor.
ΔT_m (K), minimum detectable brightness temperature contrasts (r.m.s. for 3600 s integration time at 1 MHz resolution).

Table 4. Molecular species considered in the present study

Molec. weight	Species	Observed in	To be searched in	Transitions: Millimetric ν (GHz)	Millimetric log I	Sub-millimetric ν (GHz)	Sub-millimetric log I	Far-infrared ν (GHz)	Far-infrared log I	Comments
* 2	H_2	GP, T, ISM								L, $\mu = 0$, $B = 1779$ GHz quadrupolar and pressure induced
3	HD	GP	GP					2670		L, $\mu = 7.6 \times 10^{-4}$ D, $B = 1339$ GHz
13	CH	ISM, C	GP?	191	−4.1	536	−1.5	2525	0.2	L, $\mu = 1.5$ D, $B = 425$ GHz
*14	CH_2	ISM?	GP?	68	−4.3	445	−4.5	1955	−4.0	AT, $\mu_B = 0.6$ D
*16	CH_4	GP, T, ISM	GP, T			942	−7.2	1770	−5.1	(s) SpT, $\mu = 0$, $B = 157$ GHz
17	CH_3D	GP, T, ISM	GP, T	232	−7.5	930	−5.8			SyT, $\mu_A = 0.006$ D, $B = 116$ GHz
17	NH_3	J, S, ISM	GP, T			572	−1.5	2358	−0.5	(s) SyT, $\mu_C = 1.5$ D, $B = 298$ GHz
17	OH	ISM, C, S	V, M, GP?	113	−6.5			2510	0.3	L, $\mu = 1.6$ D, $B = 556$ GHz
18	H_2O	V, M, J, SL-9/J ISM, C	GP, T	183		557	−0.8	2640	0.5	AT, (s) $\mu_B = 1.8$ D
18	NH_2D			216	−3.6	699	−2.1	2527	−0.9	AT, $\mu_C = 1.4$ D
19	HDO	V, M?, ISM	V, M	226	−3.0	600	−1.1	2598	0.1	(s) AT, $\mu_A = 0.6$ D, $\mu_B = 1.7$ D
20	HF	V	V, M, GP					1232	0.5	L, $\mu = 1.83$ D, $B = 616$ GHz
								2463	1.3	
*26	C_2H_2	GP, T, ISM								L, $\mu = 0$
26	CN	ISM, C	GP, T, I, Tr	226	−2.4	793	−1.1	1811	0.9	(s) L, $\mu = 1.4$ D, $B = 56.7$ GHz
27	HCN	N, T, SL-9/J ISM, C	GP, T	266	−1.0	354	−0.7	1770	0.2	L, $\mu = 3.0$ D, $B = 44.3$ GHz
*28	N_2	V, M, T								L, $\mu = 0$, $B = 59.6$ GHz quadrupolar and pressure induced
*28	C_2H_4	J, T, ISM, SL-9/J								AT, $\mu = 0$
28	CO	M, V, J, S, N, T SL-9/J, ISM, C	GP, T, I, Tr	230	−4.1	806	−2.7	1726	−2.4	(s) L, $\mu = 0.1$ D, $B = 57.6$ GHz
*29	$^{14}N^{15}N$		V, T							L, $\mu = ?$
29	CH_2NH	ISM	GP, T	226	−3.2	660	−2.2	2170	−1.3	(s) AT, $\mu_A = 1.3$ D, $\mu_B = 1.5$ D
*30	C_2H_6	GP, T								SyT, $\mu = 0$
30	H_2CO	ISM, C	GP, T	225	−2.3	674	−1.0	2976	−3.2	(s) AT, $\mu = 2.3$ D, $B = 38.9$ GHz
30	NO	M	M	250	−5.4	651	−3.5	1753	−3.1	(s) L, $\mu = 0.2$ D, $B = 50.9$ GHz
*31	CH_3NH_2	ISM	GP, T							AT, $\mu_A = 0.3$ D, $\mu_C = 1.2$ D magnetic dipolar transitions
32	O_2	M, V	M, V	119	−6.5	424	−6.1	1751	−6.5	(s) L, $\mu = 0$ D, $B = 43.1$ GHz
32	CH_3OH	ISM, C	GP, T	242	−3.6	331	−2.8			(s) AT, $\mu_A = 0.9$ D, $\mu_B = 1.4$ D
*32	N_2H_4		J							AT, $\mu = 0$
*32	SiH_4		J							SpT, $\mu = 0$, $A = 85.7$ GHz
33	HO_2	⊕	M, V	236	−3.4	600	−2.2	2850	−1.3	(s) AT, $\mu_A = 1.4$ D, $\mu_B = 1.45$ D
34	H_2S	ISM, C	M, V, J, S, I	216	−3.0	611	−1.9	1846	−0.6	(s) AT, $\mu_B = 0.9$ D
34	PH_3	J, S, ISM	GP	267	−3.4	800	−2.0	1863	−1.3	(s) SyT, $\mu_C = 0.6$ D, $A = 133$ GHz
34	H_2O_2	⊕	M	252	−3.0	606	−1.9	2–3000	−1.1	AT, $\mu_C = 1.6$ D
34	$^{16}O^{18}O$	ISM?								L, $\mu = 8 \times 10^{-6}$ D, $B = 40.7$ GHz

35	HCl	V, ISM	V, M, J, S			626	−1.1	2499	0.2	(s) L, $\mu = 1.1$ D, $B = 313$ GHz
40	CH_3CCH	J, T, ISM	GP, T	256	−3.1	478	−2.6			SyT, $\mu_A = 0.8$ D, $B = 8.5$ GHz
41	CH_3CN	T, ISM	GP, T	257	−2.1	606	−1.1			(s) SyT, $\mu_A = 3.9$ D, $B = 9.2$ GHz
*42	CH_3CHCH_2									AT, $\mu_A = 0.36$ D, $\mu_B = 0.05$ D
44	CS	SL-9/J, ISM, C	V, M, GP, T, I	245	−1.5	685	−0.5	1707	−1.0	(s) L, $\mu = 2.0$ D, $B = 24.5$ GHz
*44	C_3H_8	J, T, ISM	GP							AT, $\mu = 0$
44	HCP	ISM	J, S	239	−3.7	359	−3.2			L, $\mu = 0.4$ D, $B = 20.0$ GHz
44	N_2O	⊕	V, M	226	−3.8	678	−3.0	1103	−3.4	L, (s) $\mu = 0.2$ D, $B = 12.6$ GHz
44	CO_2	V, M, T, ISM, C								L, $\mu = 0$, $B = 11.0$ GHz pressure induced
44	CH_3CHO	ISM	GP, T	235	−3.0	353	−2.6			(s) AT, $\mu_A = 2.6$ D, $\mu_B = 0.9$ D
*46	$C^{16}O^{18}O$	V	V	243	−8.4	441	−7.7			L, $\mu = 7 \times 10^{-4}$ D, $B = 11.0$ GHz
46	H_2CS	ISM	GP, T	240	−2.7	652	−1.7	10–1100	−1.9	(s) AT, $\mu_A = 1.6$ D
46	NO_2	⊕, ISM	V, M	240–260	−4.5	650	−4.0	1130	−3.6	(s) AT, $\mu_B = 0.3$ D
48	SO	V, ISM	V, M, I	220	−2.3	688	−1.2	1117	−1.2	(s) L, $\mu = 1.6$ D, $B = 21.5$ GHz
*48	CH_3PH_2		S							AT, $\mu = ?$
48	O_3	⊕, M	V, M	230	−3.7	600	−3.0	1750	−2.5	(s) AT, $\mu_B = 0.5$ D
*50	C_4H_2	T	GP, T							L, $\mu = 0$
51	HC_3N	ISM, T	GP, T	263	−1.1	354	−0.9			L, $\mu = 3.7$ D, $B = 4.5$ GHz
51	ClO	⊕	V, M	241	−2.9	871	−1.9			L, $\mu = 1.2$ D, $B = 18.6$ GHz
52	HOCl	⊕	V, M	236	−3.1	619	−1.7	1780	−1.1	AT, $\mu_A = 0.4$ D, $\mu_B = 1.5$ D
*52	C_2N_2	T	GP, T							L, $\mu = 0$
55	C_2H_5CN	ISM	T	146	−3.5	860	−2.9			(s) AT, $\mu_A = 3.8$ D, $\mu_B = 1.2$ D
60	OCS	V, SL-9/J, ISM	V, M, I	243	−2.5	474	−2.2	1115	−4.0	(s) L, $\mu = 0.7$ D, $B = 6.1$ GHz
64	SO_2	V, I, ISM	V, M, I	222	−3.0	689	−2.3	1500	−1.8	AT, $\mu_B = 1.6$ D
75	HC_5N	ISM	T	223	−1.6					(s) L, $\mu = 4.3$ D, $B = 1.3$ GHz
*76	CS_2	SL-9/J								L, $\mu = 0$
*76	C_6H_6	J	GP, T							SyT, $\mu = 0$
*76	C_2N_2	T	GP, T							L, $\mu = 0$
*78	GeH_4	J, S	J, S							SpT, $\mu = 0$, $A = 80.8$ GHz
*78	AsH_3	J, S	J, S							SyT, $\mu_C = 0.2$ D, $A = 112$ GHz
80	HBr	ISM	V, M, GP			500	−1.8	2500	−0.6	L, $\mu = 0.8$ D, $B = 250$ GHz
*82	H_2Se		J, S							AT, $\mu_C = ?$
*90	AsF_3		J, S							SyT, $\mu_C = 2.8$ D, $A = 5.9$ GHz
98	H_2SO_4		V?	236	−3.1	400	−2.3			AT, $\mu_C = 2.7$ D
*128	HI		V, M, GP			385	−2.4	2306	−0.5	L, $\mu = 1.0$ D, $B = 193$ GHz

Notes:

- molecular weight of the main isotopomer; * indicates that this species is not in the JPL data base.
- ⊕, Earth; V, Venus; M, Mars; GP, giant planets; J, Jupiter; S, Saturn; U, Uranus; N, Neptune; I, Io; T, Titan; Tr, Triton; SL-9/J, impact of comet Shoemaker–Levy-9 on Jupiter; ISM, interstellar medium; C, comet(s).
- log I is the intensity parameter as defined in the JPL data base and pertains to a rotational temperature of 300 K. It is related to the line strength through: $I = 3 \times 10^{18}$ S [in cm^{-1} (molecule cm^{-2})$^{-1}$ at 300 K]. The strongest line is given in three frequency ranges: millimeter ($\nu < 300$ GHz), submillimeter (300 GHz $< \nu <$ 1 THz) and far-infrared ($\nu >$ 1 THz).
- (s) means that there are several lines of equivalent strength. L, linear; AT, asymmetric top; SyT, symmetric top; SpT, spherical top.

transitions of comparable intensities over the entire millimeter and submillimeter spectrum. This is due to the combination of a large antenna and a good atmospheric transparency. In particular, this type of instrumentation is best suited for small objects having very large dilution factors. Triton and Pluto, unfortunately, appear to be beyond the limit of the heterodyne technique. In any case, if a molecule is observable below 300 GHz, observations at higher frequencies should be considered only when the gain in line intensity is of at least a factor of 10, or when spatial resolution is needed.

(2) A comparison of the CSO and FIRST cases shows that, when the planet fills the FOV, or at least a large fraction of it (as is the case of Venus, Mars, Jupiter, and Saturn), the maximum sensitivity is reached with FIRST, due to its very low system temperature. For small objects (Uranus, Neptune, Titan, and Io), the large dilution factor of FIRST counterbalances the low value of T_{sys}, so that, in the atmospheric windows observable from the ground, the performances of the CSO and FIRST are comparable. Of course FIRST is unique for all transitions unobservable from the ground, in particular H_2O and O_2.

Finally, it should be noted that the minimum detectable brightness temperature contrasts are calculated under the assumption that the observed spectra have flat baselines, not affected by ripples. Experience shows that this is not always the case, especially for strong sources like Venus, Mars, Jupiter, and Saturn. This restriction has to be kept in mind when final conclusions are drawn.

4. Selection of molecules

Our selection of molecules was based on the following criteria. We have first considered all molecules already detected in a planetary or satellite atmosphere, and we have analyzed their possible detectability in other objects. We have added in our list all molecules whose presence in a planetary atmosphere has been suggested from theoretical modelling or simulation experiments. Finally we have also considered the list of known interstellar molecules. As a baseline, we have used the compilation of molecules, radicals and ions made by Crovisier (1993). Table 4 summarizes all the species which have been considered in the present study, and gives information about their rotational structure, with examples of typical line intensities in various spectral ranges. A unique rotational temperature of 300 K was adopted, which is intermediary between that of the outer planets and that of Venus' lower atmosphere. In this table, isotopes of a given species have been considered only for the most abundant molecules, and when their rotational structure differs from the one of the given species. The list given in Table 4 is probably not exhaustive, but should include most of the species of planetary interest for which spectroscopic information is known.

For estimating the possible abundance of a given species in a planetary atmosphere, we have used the following references. In the case of Venus, we have used the analyses of Von Zahn *et al.* (1983), Krasnopolsky and Parshev (1983), and Krasnopolsky (1986). For Mars we have used the review by Krasnopolsky (1986). In the case of the giant planets, we have used the work of Lellouch and Destombes (1985), Bézard *et al.* (1986), and reviews by Atreya (1986) and Encrenaz (1990). For Titan, our work is based upon the review of Hunten *et al.* (1984), the laboratory work by Cerceau *et al.* (1985) and Raulin *et al.* (1990), and the synthetic calculations of Coustenis *et al.* (1993). In the case of Io we have used Lellouch *et al.* (1992), and for Triton and Pluto we have used Lunine *et al.* (1989).

In our analysis, we have considered, for each planet or satellite, all species which might have at least a small probability of being present, on the basis of our current knowledge. In the final discussion (Section 6), as a general rule, we have selected, for each object, all molecules expected to be present above the 10^{-10} mixing ratio level, and all species for which a significant upper limit could be expected. In addition, in order to make this study as complete as possible, we have also considered a few species which are less likely to be detectable, but for which little information is known. On the basis of general photochemical models, we have added some oxygen, carbon and sulfur compounds in the case of the terrestrial planets, and we have included some hydrogenated species, hydrocarbons and nitriles in the giant planets and Titan. With the exception of CO_2 on Venus (abundant enough for its pressure-induced spectrum to be significant), we have not discussed molecules with no dipole moment, as they have no rotational transitions.

5. Modelling

Nominal thermal profiles have been chosen for all planets and satellites, following the work of Seiff (1983) in the case of Venus, Krasnopolsky (1986) for Mars, Gautier and Owen (1989) for Jupiter, Saturn and Uranus, Conrath *et al.* (1987) for Neptune, Hunten *et al.* (1984) and Lellouch *et al.* (1989) for Titan. In the case of the other satellites, there is a large uncertainty about the temperature distribution; these cases are discussed separately in Section 6.4. Vertical temperature and pressure profiles are shown in Figs 9–15. With the exception of a few specific cases mentioned in the text (H_2O and HDO on Mars and Venus, in particular), the mixing ratios are assumed to be constant with altitude.

Our modelling assumes a uniform distribution of temperature and abundances over the planetary disk. This is a first approximation, sufficient for the purpose of estimating detectability limits. However, non-uniformity might be a dominant effect for some species, due to pole–equator or day–night variations.

Our radiative transfer model has been described in Lellouch *et al.* (1989, 1991a). The planetary atmosphere is divided into about 200 layers. Opacities are calculated at each atmospheric layer at 256 different frequencies covering the range ($\nu_0 - 0.25$ GHz, $\nu_0 + 0.25$ GHz), with a variable step (from 0.1 GHz, far from the center, to 0.1 MHz at the line center). The outgoing flux is integrated over all altitudes, either at the disk center or over the whole disk, taking into account the limb contribution. A Voigt profile

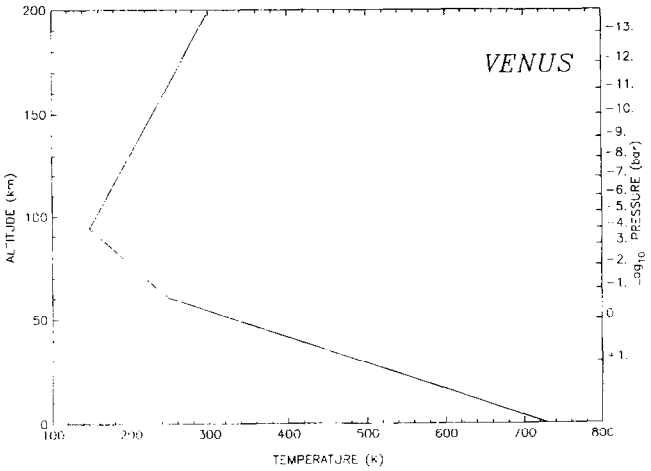

Fig. 9. Nominal thermal profile of Venus (after Seiff, 1983)

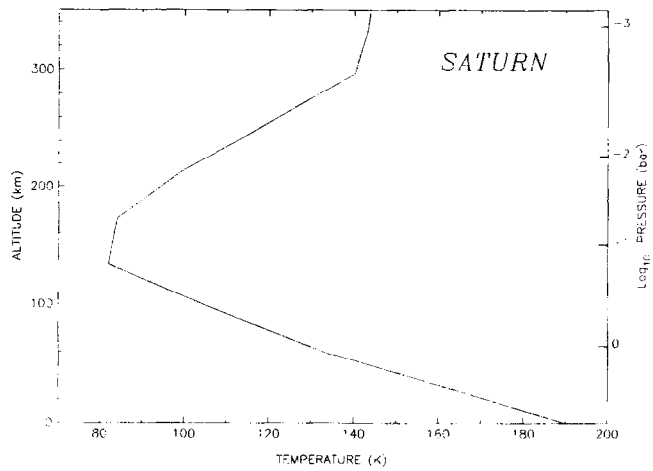

Fig. 12. Nominal thermal profile of Saturn (after Gautier and Owen, 1989)

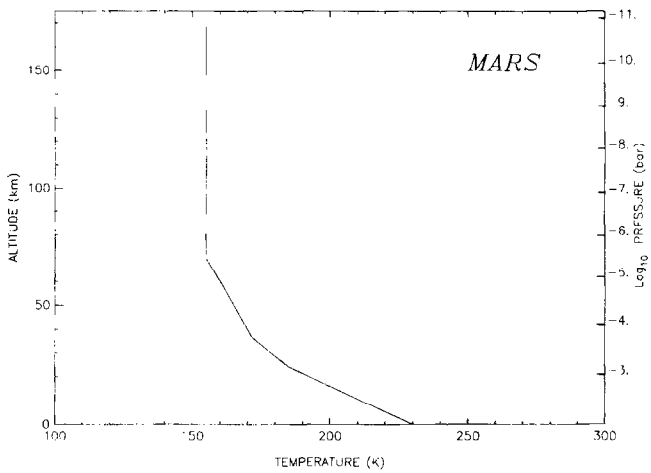

Fig. 10. Nominal thermal profile of Mars (after Krasnopolsky, 1986)

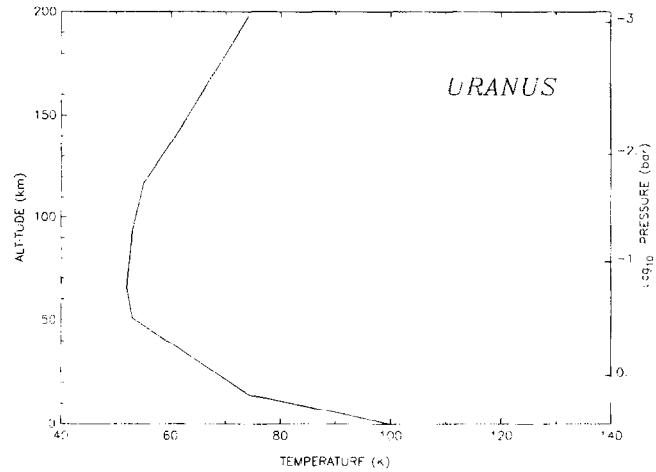

Fig. 13. Nominal thermal profile of Uranus (after Gautier and Owen, 1989)

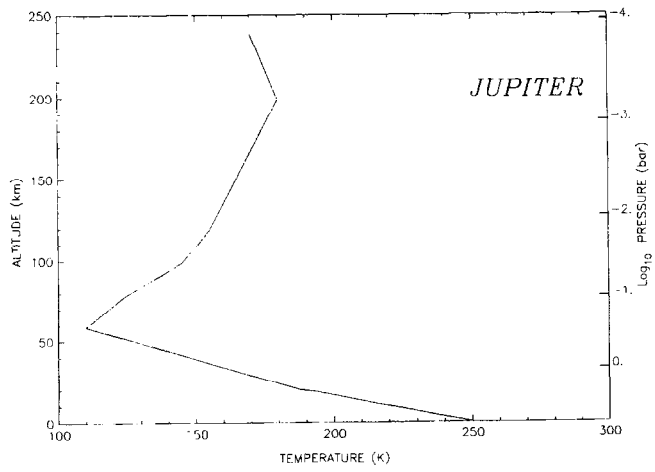

Fig. 11. Nominal thermal profile of Jupiter (after Gautier and Owen, 1989)

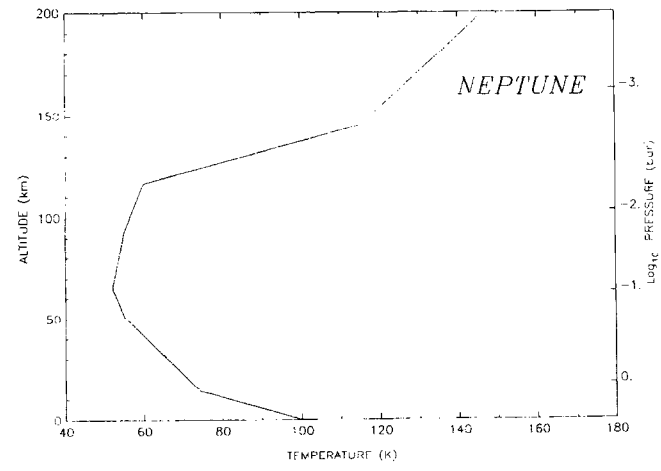

Fig. 14. Nominal thermal profile of Neptune (after Gautier *et al.*, 1995)

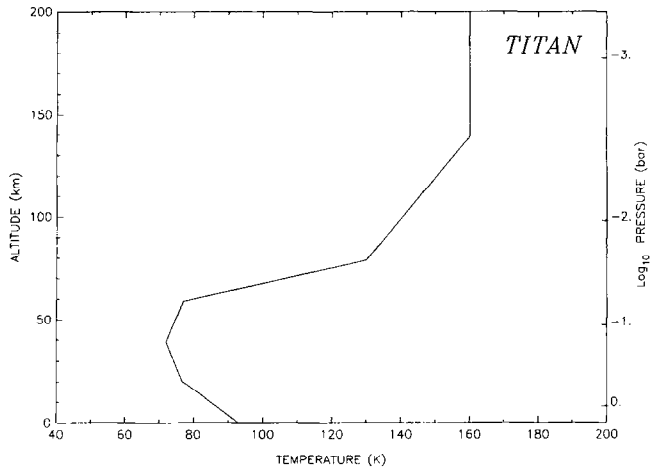

Fig. 15. Nominal thermal profile of Titan (after Hunten *et al.*, 1984)

is used to account for the Doppler regime in the upper planetary atmospheres. In the case of Mars, we treated the planet as a dielectric sphere with uniform surface temperature, with an averaged surface emissivity of 0.90 (dielectric constant = 2.5).

Spectroscopic constants (line position, strength and Lorentz-broadening) were mostly taken from the Poynter and Pickett catalog (Poynter and Pickett, 1984; Pickett *et al.*, 1992) and the GEISA databank (Husson *et al.*, 1986). Whenever possible, improved values of the pressure-broadening coefficients were used, taking into account the major atmospheric gas responsible for the broadening (CO_2 for Venus and Mars; H_2 for the giant planets; N_2 for Titan).

The pressure-induced absorption was calculated according to the following formulae (ν in cm^{-1}, n in amagat):

- For Venus (CO_2–CO_2 collisions)

$$\alpha_{CO_2\text{-}CO_2} = 1.7 \times 10^{-10} \nu^2 n^2_{CO_2}. \quad (12)$$

- For the giant planets (H_2–H_2 and H_2–He collisions)

$$\alpha_{H_2\text{-}H_2} = 1.0 \times 10^{-10} \nu^2 n^2_{H_2} \quad (13)$$

$$\alpha_{H_2\text{-}He} = 1.6 \times 10^{-10} \nu^2 n_{H_2} \cdot n_{He}. \quad (14)$$

The H_2/He ratios were taken from Gautier *et al.* (1981) (Jupiter), and Conrath *et al.* (1984, 1987, 1991) (Saturn, Uranus and Neptune).

- For Titan (N_2–N_2 collisions)

$$\alpha_{N_2\text{-}N_2} = 4.0 \times 10^{-9} \nu^2 n^2_{N_2}. \quad (15)$$

Our calculations are in general agreement, with previous synthetic spectra modelled at lower spectral resolution, in the far-infrared range, in the case of giant planets (Lellouch *et al.*, 1984a; Bézard *et al.*, 1986) and Titan (Coustenis *et al.*, 1993). They are also consistent with high-resolution synthetic spectra of Titan in the millimeter range (Paubert *et al.*, 1984).

In what follows, the synthetic planetary spectra have been calculated (in brightness temperature units) for the entire disk, over a 0.5 GHz interval with a resolution of 1 MHz, to fit the nominal conditions of heterodyne spectroscopy measurements. In a few cases, the spectral range has been extended up to 5 GHz to allow a comparison with ISO observations; in the case of very narrow lines (Io, Titan), the spectral resolution has been lowered to 100 kHz. The brightness temperature unit is directly comparable to the minimum brightness temperature differences calculated in Table 3. The detectability limits indicated below correspond to a 1-sigma limit for 1 h of integration time and a spectral resolution of 1 MHz. We note that, for a reliable detection, a S/N > 3 is necessary; we can also mention that, in most of the cases, the expected line-widths are larger than 1 MHz, so that the r.m.s. can be decreased by degrading the spectral resolution.

6. Results

The main results of the present study are summarized in Tables 5 (Venus), 6 (Mars) and 7 (giant planets and Titan).

6.1. *Venus*

6.1.1. O_2 *and oxygen-bearing molecules.* O_2. The abundance of oxygen in the atmosphere of Venus has been a matter of controversy. An O_2 airglow was observed by Connes *et al.* (1979); it is probably caused by the recombination of O atoms produced on the dayside by CO_2 photolysis. *Pioneer Venus* experiments (Oyama *et al.*, 1980) derived a mixing ratio of several tens of ppm in the 40–50 km range, but a much lower limit was derived by other means (Traub and Carleton, 1974), so that the O_2 detection remains questionable.

If oxygen were present in the Venus atmosphere with a constant mixing ratio of 50 ppm, its spectroscopic detection would be possible with FIRST, if Venus is observable with this satellite despite its small solar elongation. The best transition lies at 424 GHz and the temperature contrast would be 1.5 K (Fig. 16). A S/N of 50 could then be achieved in 1 h integration time. However, as mentioned above, such an oxygen abundance is unlikely. The detectability limit corresponding to this line is thus 1 ppm in 1 h. It can be noted that another transition, slightly weaker, lies at 119 GHz.

Another way to search for O_2 in Venus would be to study its isotopic transition $^{16}O^{18}O$ at 234 GHz. Still for an oxygen mixing ratio of 50 ppm, the temperature contrast is 0.05 K. Its detection at this level would require several hours of integration time at IRAM.

O_3. Ozone has not been observed on Venus. Theoretical photochemical models by Krasnopolsky and Parshev (1983) predict a vertical distribution with mixing ratios of 10^{-11} at 80 km and 10^{-7} at 100 km and above.

Using this distribution, and the 610 GHz transition, we obtain a brightness temperature contrast of 0.8 K, which should be detectable at CSO with a S/N of 5 in 1 h integration (Fig. 17).

Another strong transition is present at 239 GHz. The

Table 5. Observability of rotational transitions on Venus and detectability limits

Species	Det?	A	B	C	D	E	F	Comment
O_2	Y			D? (424)				• Controvers. abundance • Assumed: 50 ppm
$^{16}O^{18}O$	N	MD? (234)						
O_3	P	MD	D (610)					• Assumed: 10^{-11} (80 km) 10^{-7} (100 km)
H_2O	Y	O (183)		D (557)			D	• $H_2{}^{17}O$ and $H_2{}^{18}O$ also detectable
HDO	Y	O (226)		D (600)				
H_2O_2	N	10^{-9} (606)						• Detection not expected
HO_2	N	10^{-9} (611)						• Detection not expected
CO	Y	O (115, 230)						• Isotopes also observed
CO_2	Y							• Pressure induced cont.
$C^{16}O^{18}O$	Y	MD (243)						
H_2CO	N	2×10^{-10} (225)	10^{-10}					• Detection unlikely
SO	Y	MD (220)	D (689)					• Assumed: 3×10^{-9} (60 km) 10^{-10} (70 km), 5×10^{10} (>80 km)
SO_2	Y				D?			• Present in lower atm.
H_2S	Y				D?			• Present in lower atm.
OCS	Y				D?			• Present in lower atm.
CS	N		10^{-10} (636)					
H_2SO_4	P							• Depleted by saturation above the clouds
$^{14}N^{15}N$	N							• Rot. trans. too weak to be observable
NO	Y		3×10^{-7} (651)					• Located above 100 km, detection not expected
CN	N	2×10^{-10} (226)						• Detection not expected
NH_3	N			10^{-10} (572)				
HCl	Y		D (626)				D	• Assumed 4×10^{-7} $H^{37}Cl$ also detectable
ClO	P	10^{-8} (241)						• Detection not expected
HF	Y						D	
HBr	N						D	
HI	N						D	

Notes: The numbers refer to constant mixing ratios throughout the atmosphere. Y, detected; N, not detected; P, predicted; O, observed in rotational lines; D, detectable; MD, marginally detectable.

expected contrast, with the same vertical distribution, is 0.16 K, which could be detectable at IRAM.

H_2O. Water vapor has been detected on Venus, both on the night side and on the day side. Below the clouds, at altitudes lower than 50 km, the H_2O mixing ratio is about 30 ppm (Von Zahn *et al.*, 1983; Bézard *et al.*, 1990; de Bergh *et al.*, 1995). Above the clouds, it seems to show spatio-temporal variations. Because the H_2O distribution is constrained by saturation, its observation in the millimeter range can provide information upon both the water vapor abundance and the temperature of the mesosphere where the line is formed (z = 95 km).

H_2O has been recently detected at 183 GHz at IRAM (Encrenaz *et al.*, 1995a). However, this transition can be observed only under exceptional weather conditions. The most favorable transition for submillimeter spectroscopy is the 557 GHz transition (Fig. 18). The very large temperature contrast (50 K) will be easily observable with FIRST, or even a smaller space satellite (such as ODIN) having comparable instruments. Observing the line core

Table 6. Observability of rotational transitions in Mars and detectability limits

Species	Det?	A	B	C	D	E	F	Comments
O_2	Y			D (424)				• Assumed: 1.3×10^{-3}
$^{16}O^{18}O$	N	D (234)						
O_3	Y	D? (239)	D? (610)					• Strong seasonal effect
H_2O	Y	O (22, 183)		D (557)		D	D	• Strong seasonal effect
HDO	Y	O? (226)	D (600)			D	D	
H_2O_2	P	D? (252)	D (606)					
HO_2	N	10^{-9} (611)						
CO	Y	O (115, 230)	O (345)					• Isotopes also observed
H_2CO	Y?		10^{-10}					• Controv. detection
SO	N		10^{-10} (689)					
SO_2	N		10^{-9} (689)					
H_2S	N		10^{-9} (611)					
OCS	N	10^{-9} (243)						
CS			10^{-10} (636)					• Detection unlikely
NO	Y	D? (250)	D (651)					• Assumed: 5×10^{-6} (100–300 km)
NH_3	N			10^{-10} (572)				• Detection unlikely
CN	N	2×10^{-10} (226)						• Detection unlikely
HCl	P?		D? (626)		D?	D?	D?	• Assumed: 4×10^{-7} • $H^{37}Cl$ also detectable
ClO	N	10^{-8} (241)						
HBr	N		D? (500)				D?	
HI	N		D? (385)				D?	

See Notes to Table 5.

at high spectral resolution (100 kHz) could even permit the retrieval of the thermal profile above the minimum temperature level, if a temperature inversion takes place. Transitions of $H_2{}^{18}O$ and $H_2{}^{17}O$ will be observable with FIRST as well.

Unfortunately, Venus will not be observable with the ISO satellite, because of the constraint on solar elongation angle. Without this constraint, several H_2O rotational lines would have been easily detectable in the far-infrared range.

HDO. The HDO detection is relatively easy on Venus, thanks to the very strong deuterium enrichment (about 120 times the terrestrial value) on this planet (de Bergh *et al.*, 1991). HDO has been detected at 226 GHz at IRAM (Encrenaz *et al.*, 1991a). However, this transition is weak, and the observed temperature contrast is 1.5 K.

A much more favorable transition lies at 600 GHz: the expected temperature contrast is 50 K (Fig. 19). Its observation, easily feasible at CSO, will allow a better determination of the H_2O content (assuming that the D/H ratio on Venus is known) and a better constraint on the mesospheric temperature.

It should be noted that a simultaneous observation of H_2O and HDO with FIRST will allow a new determination of the D/H ratio on Venus, independent of the previous near-infrared spectroscopic measurements.

H_2O_2. According to Krasnopolsky and Parshev (1983), the vertical distribution of H_2O_2 is expected to peak at an altitude of 80 km, with a number density less than 10^5 cm^{-3}, corresponding to a mixing ratio smaller than 10^{-11}. If this model is correct, its detection on Venus is impossible. The most favorable H_2O_2 transition, at 606 GHz,

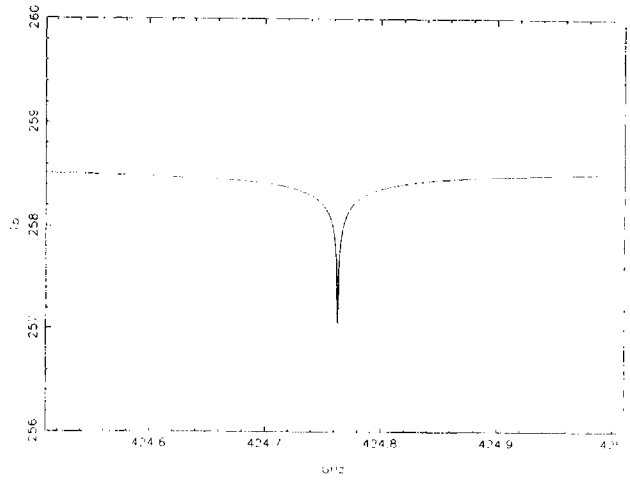

Fig. 16. The synthetic spectrum of O_2 on Venus (424 GHz). The assumed O_2 mixing ratio is 5×10^{-5} (constant with altitude)

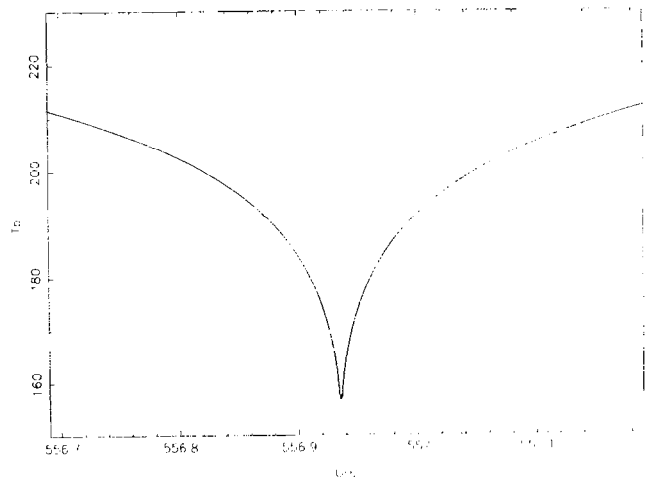

Fig. 18. The synthetic spectrum of H_2O on Venus (557 GHz). The assumed H_2O mixing ratio is 4×10^{-5} at 55 km, 3×10^{-6} at 65 km, and is constrained by saturation above 65 km (see Encrenaz *et al.*, 1991a, 1995a)

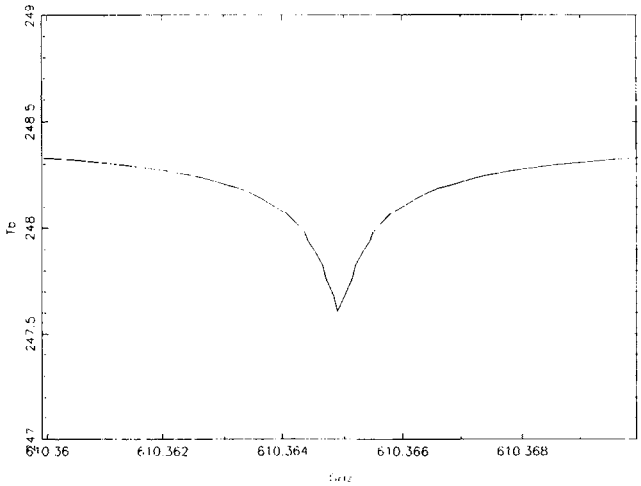

Fig. 17. The synthetic spectrum of O_3 on Venus (610 GHz). The assumed O_3 mixing ratio is 10^{-7} at $z = 100$ km (see text)

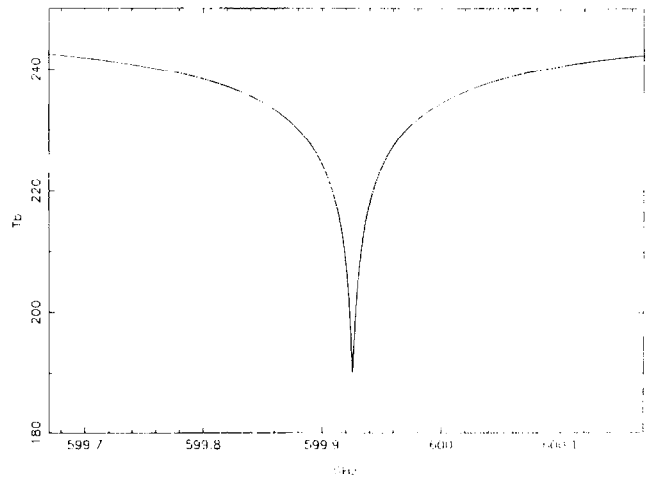

Fig. 19. The synthetic spectrum of HDO on Venus (600 GHz). The assumed H_2O mixing ratio is the same as in Fig. 18. The D/H ratio in Venus is assumed to be 120 times the terrestrial value, i.e. 0.018

would lead to a detectability limit in the range of 10^{-9} with the CSO.

HO_2. Theoretical calculations by Krasnopolsky and Parshev predict a HO_2 abundance peak at 85 km with a number density of 10^7 cm^{-3}, which corresponds to a mixing ratio of 10^{-10} at this level.

HO_2 could be searched for at 611 GHz, where a detectability limit of 10^{-9} (constant mixing ratio) could be achieved. Thus, this upper limit would not be very stringent.

OH. The OH abundance, according to models, is expected to peak at 95 km with a mixing ratio below 10^{-10}. The rotational transitions of OH, which are in the far-infrared, are not observable presently with enough spectral resolution. Thus, the detection of OH on Venus does not look feasible by the technique described here.

6.1.2. *Carbon-bearing molecules.* CO. CO was the first molecule to be detected on Venus (Kakar *et al.*, 1976). Its vertical distribution has been inferred, with the mesospheric temperature, and the CO temporal variations have been monitored over more than a decade by various authors (e.g. Clancy and Muhleman, 1985). ($J = 1$–0) and ($J = 2$–1) transitions of CO and its isotopes have been observed. CO measurements have also been used for measuring wind velocities over the Venus disk (Pierce *et al.*, 1991).

In the temperature range of the Venus mesosphere, the CO lines of maximum intensity occur around a frequency of 1 THz. However, their observation would give little advantage, as compared to the present observations, except a better spatial resolution for the CO and thermal mapping, and the wind velocity measurements. Even in this case, observing CO lines around 1 THz at CSO will provide little improvement with respect to IRAM

Table 7. Observability of rotational transitions in giant planets and Titan and detectability limits

Species	Det?	A	B	C	D	E	F	Comments
CH_4	Y		D (J,S) (942)			D (GP,T)	D (GP,T)	• Sci.obj.: T(P) (J,S) CH_4(U,N,T)
CH_3D	Y		D? (J,T) (930)					
C_3H_4	N(GP) Y(T)	10^{-8}(J,S) 3×10^{-7}(N) 2×10^{-6}(T) (257)						• Mix.rat. in T: 2×10^{-6}
CH	N		10^{-10}(J,S) 3×10^{-9}(N) 2×10^{-8}(T)					• Detection not expected
CH_2	N	4×10^{-10}(J,S) 10^{-8}(N) 10^{-7}(T) (68)						• Detection not expected
NH_3	Y(GP)			10^{-10}(J) 3×10^{-9}(N) 2×10^{-8}(T) (572)				• Observed in J&S troposph. • Det. limits are for N&T strat.
HCN	Y (J?,N,T, SL-9/J)	O(N,T) (264)	O(N) (352)		D (J,S)	D	D	• Troposph. on J • Strat. on N&T
CH_3CN	Y(T)	O(T) 10^{-9}(J) 3×10^{-8}(N) (257)	D(T) (606)					
HC_3N	Y(T)	O(T) 10^{-10}(J) 3×10^{-9}(N) (263)						
CH_2NH	N	10^{-8}(J) 3×10^{-7}(N) 2×10^{-6}(T)						
CN	N	10^{-10}(J,S) 3×10^{-9}(N) 2×10^{-8}(T)						• Detection not expected
CO	Y (J,S,N,T, SL-9/J)	O(N,T) (115,230)	O(N) (345)		D (J,S,T)	D	D	• Trop. on J&S • Strat. on N&T
H_2O	Y(J) P(S,T)			D(S,T) (557)				• Trop. on J • Predicted in S&T stratosph.
H_2CO	N			10^{-10}(J,S) 3×10^{-9}(N) 2×10^{-8}(T) (674)				• Detection not expected
CH_3OH	N	10^{-8}(J,S) 3×10^{-7}(N) 2×10^{-6}(T)						• Detection not expected
HD	Y(GP)				D(GP)			• Sci.obj.: D/H
PH_3	Y(J,S)	3×10^{-8}(J,S) (267)			D	D	D	• Trop. on J&S
HCl	N		D(J,S) (626)		D(J,S)	D (J,S)	D (J,S)	• Assumed: 4×10^{-7} • $H^{37}Cl$ also det.
HF	N					D (J,S)	D (J,S)	
HBr	N		D(J,S)? (500)		D(J,S) (?)	D (J,S)	D (J,S)	
HI	N		D(J,S)? (385)		D(J,S) (?)	D (J,S)	D (J,S)	

Table 7. (*Continued*)

Species	Det?	A	B	C	D	E	F	Comments
H_2S	N P(J)				D(J)?	D(J)?	D(J)?	
CS	Y(SL-9/J)	2×10^{-11}(J,S) 6×10^{-10}(N) 4×10^{-9}(T)						• Detection not expected under normal conditions
OCS	Y(SL-9/J)	2×10^{-10}(J,S) 6×10^{-9}(N) 4×10^{-8}(T)						• Detection not expected under normal conditions
HCP	P(S)				D(S)?	D(S)?	D(S)?	• Assumed: 10^{-8}
H_2Se	N				D?	D?	D?	• Assumed: 10^{-9}
	P(J,S)				(J,S)	(J,S)	(J,S)	(troposph.)
AsF_3	N				D?	D?	D?	• Assumed:
	P(J,S)				(J,S)	(J,S)	(J,S)	4×10^{-10} (trop.)

See Notes to Table 5.

measurements at 230 GHz. In addition, millimeter interferometry appears better suited for this type of study.

CO_2. Carbon dioxide has no dipole moment, but contributes to the millimeter spectrum of Venus through its pressure-induced continuum, which, at 230 GHz, limits the penetration level to the cloud level.

The $C^{16}O^{18}O$ isotope of carbon dioxide was detected in the IR range by Bézard *et al.* (1987); it also presents weak rotational transitions. Assuming a solar value for $^{16}O/^{18}O$, i.e. a mixing ratio of 4×10^{-3}, the 243 GHz transition ($J = 11$–10) gives a temperature contrast of 0.5 K, which might be detectable at IRAM; the 441 GHz transition ($J = 20$–19) gives a contrast of 2.5 K, which could be detectable with the CSO. The scientific interest of this detection would be to map the temperature field of the Venus night side near the cloud top at the time of inferior conjunction.

H_2CO. There is presently no information about what could be the H_2CO content on Venus. Formaldehyde is believed to be formed either by CH_4 oxidation, or by H_2O–CO heterogeneous reactions. From what we know now, methane does not exist in the Venus atmosphere, and both CO and H_2O are present in very weak amounts. The detection of H_2CO on Venus appears very unlikely.

H_2CO exhibits very strong rotational transitions. The most appropriate range to search for this species would be 600–700 GHz, using the CSO. The expected detectivity limit would correspond to a constant mixing ratio in the range of 10^{-10}.

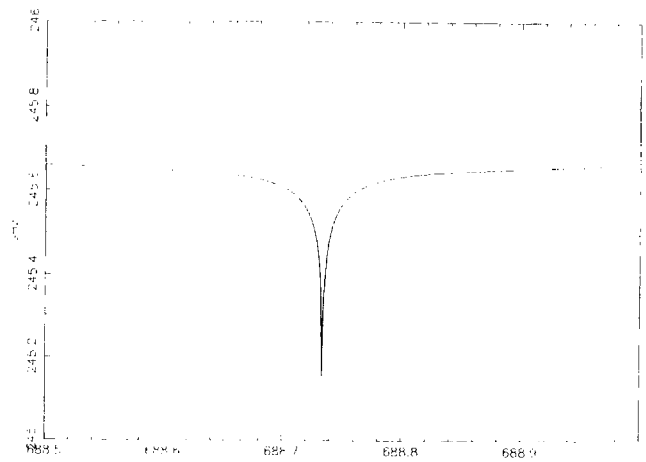

Fig. 20. The synthetic spectrum of SO on Venus (688.7 GHz). The assumed SO mixing ratio is 3×10^{-9} at $z = 60$ km (see text)

6.1.3. *Sulfur-bearing molecules.* SO. SO has been detected on Venus in the UV range (Na *et al.*, 1990). However, theoretical photochemistry models predict that the SO mixing ratio might reach 3×10^{-9} at $z = 60$ km (Krasnopolsky and Parshev, 1983), decrease down to 10^{-10} at 70 km, and stay around 5×10^{-10} above 80 km.

SO has a large number of very strong rotational transitions. Among others, a good candidate is the 689 GHz transition, observable from the ground. We calculate a temperature contrast of 0.5 K (Fig. 20) which could be detectable at CSO with a S/N of 3 in 1 h of integration time. The 220 GHz transition would be also marginally detectable at IRAM.

SO_2. Sulfur dioxide has been detected at various levels of the Venus atmosphere. Its mixing ratio is about 150 ppm below the clouds (22 km $< z <$ 50 km), but decreases within the clouds to a value of about 0.05 ppm at 70 km, because of its conversion to H_2SO_4 (Von Zahn *et al.*, 1983; Bézard *et al.*, 1993b).

The SO_2 molecule is spectroscopically very active, and shows a forest of very strong transitions. As an example, the 689.4 GHz line leads to a temperature contrast of 0.5 K between the center and the edge of the 0.5 GHz bandwidth. However, as shown in Fig. 21, the line calculated with the vertical distribution mentioned above is too broad to be observed by heterodyne spectroscopy.

In contrast, the search for SO_2 on Venus might be a possible objective for ground-based Michelson interferometry (case D). The temperature contrast between the SO_2 line center and the true continuum (as observed in Fig. 20 for a nearby frequency) is 1.2 K, corresponding to a line depth of 0.5%. A S/N higher than 200 would thus be required to detect the line, which may not be impossible on a strong source like Venus.

H_2S. Hydrogen sulfide is also present in the lower atmosphere of Venus, and destroyed at the cloud level, with mixing ratios ranging from 3 ppm below 20 km down to 1 ppm at 55 km. H_2S has strong rotational transitions throughout the millimeter and submillimeter; interesting

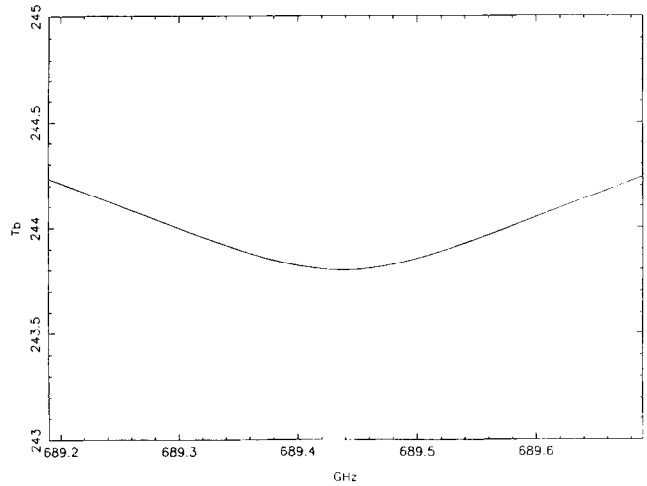

Fig. 21. The synthetic spectrum of SO_2 on Venus (689.4 GHz). The assumed SO_2 mixing ratio is 5×10^{-8} at $z = 70$ km (see text)

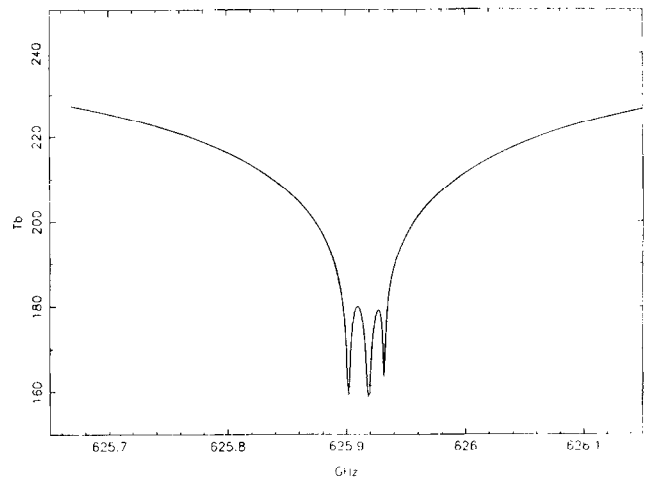

Fig. 22. The synthetic spectrum of $H^{35}Cl$ on Venus (626 GHz). The assumed $H^{35}Cl$ mixing ratio is 4×10^{-7} (constant with altitude)

transitions appear, in particular, at 216 and 611 GHz. As for SO_2, H_2S transitions are likely to be too broad to be detectable with heterodyne spectroscopy; the detectability limit would correspond to a constant mixing ratio of about 10^{-9}. Like SO_2, H_2S could be searched for with ground-based Fourier-transform spectroscopy.

OCS. Carbonyl sulfide presents the same characteristics as the two previous sulfur-bearing molecules, SO_2 and H_2S: it is present in the lower atmosphere with a mean mixing ratio of about 0.5 ppm near 37 km (Bézard *et al.*, 1990), but its abundance decreases as the altitude increases (Pollack *et al.*, 1993), and OCS is destroyed at the cloud level.

Like SO_2 and H_2S, OCS shows many rotational transitions, which would lead to lines too broad to be detectable with heterodyne spectroscopy. In particular, the 243 GHz transition, observed with IRAM leads to a detectability limit in the range of 10^{-9}. OCS could be searched for with ground-based Fourier-transform spectroscopy.

CS. There is no information about the CS radical. Its presence is not expected from theoretical grounds.

Using the CSO, the detectability limit for a constant mixing ratio would be 10^{-10} from the 636 GHz transition.

H_2SO_4. The H_2SO_4 water vapor is relatively abundant just below the cloud level (a few ppm at $z = 50$ km, according to Krasnopolsky and Parshev (1983)), but is constrained by saturation above this level. Its detection is thus not possible with heterodyne spectroscopy, for the same reasons as mentioned above in the case of SO_2, H_2S and OCS. In addition, in the case of H_2SO_4, the lines would probably be formed below the level of the CO_2–CO_2 continuum, which would make them disappear independently of their linewidth.

6.1.4. *Nitrogen-bearing molecules.* N_2. Nitrogen is spectroscopically inactive. Its isotope $^{14}N^{15}N$, however, has weak rotational transitions, but the N_2 abundance in Venus (3.5%) is too small for these lines to be detectable.

NO. A nitric oxide airglow was observed by the *Pioneer Venus* and *IUE* (International Ultraviolet Explorer) UV spectrometers, and its origin was explained by reactions on N and O in the 80–140 km range. However, the amount of nitrogen atoms in the Venus atmosphere (maximum of 10^8 at $z = 115$ km (Krasnopolsky, 1986), which corresponds to a mixing ratio of 10^{-5} at this level) is not sufficient to form enough NO for a detectable signature in the millimeter range.

NO exhibits two series of multiplets at 250 and 650 GHz, and the transitions are rather weak. At 651 GHz, the detectivity limit would correspond to a constant mixing ratio of 3×10^{-7} (case B), which is likely to be meaningless.

NO_2 and N_2O. There is no information nor prediction about the abundances of these species in the Venus upper atmosphere. Furthermore, taking into account the low abundance of NO and the weak intensities of the NO_2 and N_2O transitions (see Table 4), the detection of these species in Venus is not expected.

CN. There is no information about the CN abundance on Venus. However, it can be noted that CN has strong rotational transitions, which could lead to a detectability limit in the range of 2×10^{-10} with IRAM (case A).

NH_3. An upper limit of 3×10^{-8} was obtained for the NH_3 mixing ratio in the lower atmosphere from ground-based near-IR spectroscopy (Kuiper, 1968). Titov (1983) suggested that ammonia might still be present in lower abundance and react with SO_2 in the clouds to form ammonium pyrosulfite $(NH_4)_2S_2O_5$, but there is no confirmation of this model.

Heterodyne spectroscopy could allow to refine the NH_3 upper limit above the clouds, from the observation of the strong $J = 1$–0 transition of ammonia at 572 GHz. As this line is not accessible from the ground, this observation would have to be done from space. An upper limit of 10^{-10} could be reached with FIRST in 1 h observing time (case C).

6.1.5. HCl, *other* Cl*-bearing molecules and other halides.* HCl. HCl was discovered by ground-based near-IR spectroscopy (Connes *et al.*, 1967), above the clouds, with a mixing ratio of 4×10^{-7}. The same value was measured in the lower atmosphere on the night side (Bézard *et al.*, 1990).

If the HCl mixing ratio is constant throughout the Venus atmosphere, its detection with heterodyne spectroscopy is expected to be very easy. Indeed, HCl exhibits

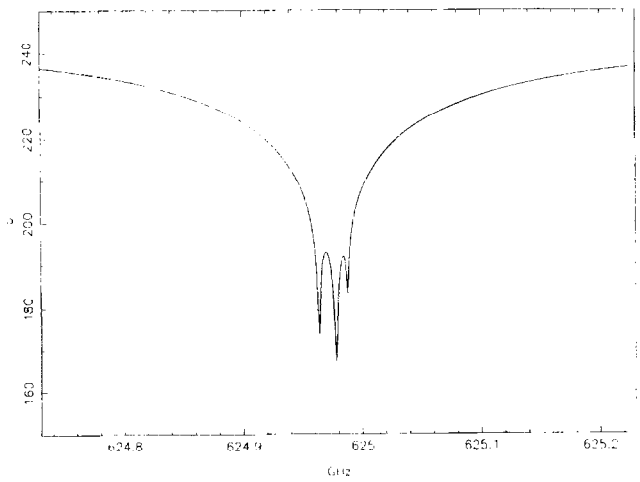

Fig. 23. The synthetic spectrum of $H^{37}Cl$ on Venus (625 GHz). The assumed $H^{35}Cl$ (constant) mixing ratio is 4×10^{-7}. The $^{37}Cl/^{35}Cl$ ratio is 0.325

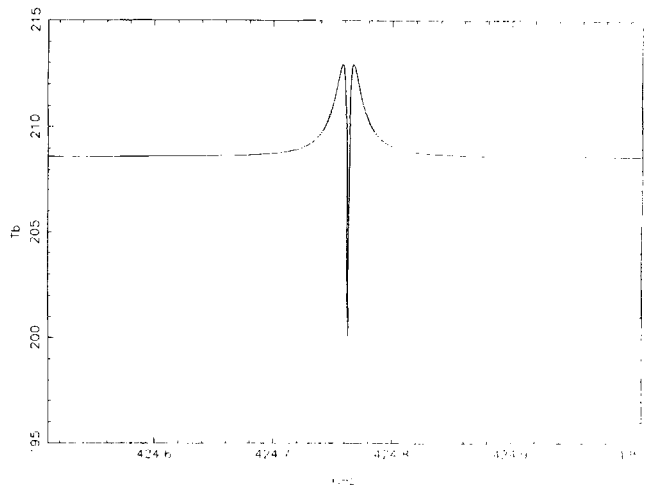

Fig. 24. The synthetic spectrum of O_2 on Mars (424 GHz). The assumed O_2 mixing ratio is 1.3×10^{-3} (constant with altitude)

a multiplet at 626 GHz, while its isotope $H^{37}Cl$ shows the same multiplet shifted by 1 GHz at 625 GHz. Assuming the cosmic value of 3.1 for the $^{35}Cl/^{37}Cl$ ratio (Anders and Grevesse, 1989), the two multiplets would be easily detectable (Figs 22 and 23). This observation should be feasible at CSO in the near future. In the case of a constant vertical distribution, the expected line contrast would be about 50 K, so that a S/N higher than 100 should be achieved in less than 10 min.

HCl, however, might be photodissociated in the upper atmosphere of Venus, as suggested by several authors, and be responsible for the hydrogen escape and the recombination of CO and O_2 (Prinn, 1973). In this case, it should be noted that the multiplet structure of the transition will allow a precise retrieval of the HCl vertical distribution.

Finally, the search for HCl could also be tempted using a ground-based interferometer (case D); however, the spectral resolution would not be sufficient to separate the multiplets and to retrieve the vertical distribution.

ClO. Theoretical models of chlorine chemistry predict the formation of ClO as a result of the HCl photodissociation and the reaction of Cl atoms with HO_2 (Krasnopolsky and Parshev, 1983). The ClO density would reach a maximum of 10^8 cm^{-3} at 80 km, which corresponds to a mixing ratio of 10^{-9} at this level.

ClO has a large number of strong transitions throughout the millimeter and submillimeter range. As an example, the 241 GHz transition, accessible with IRAM, would provide a detectability limit corresponding to a constant mixing ratio of about 10^{-8} (case A). This limit is thus probably not very useful.

HF and other halides. As HCl, HF has been detected in the near-infrared range (Connes *et al.*, 1967; Bézard *et al.*, 1990); its mixing ratio was found to be 10^{-9} above the clouds as well as in the deep atmosphere.

HF has very strong rotational transitions, all in the far-infrared range. The first transition ($J = 1$–0) lies above 1.2 THz. Its observation could be attempted with a Fabry–Pérot spectrometer from space (case F), as, for example, FIRST, if Venus is observable with this satellite. The same comment applies to HBr and HI, although expected to be present in lower abundances. It should be mentioned that HBr and HI have their first rotational transitions at 500 and 385 GHz, respectively, possibly observable from the ground with heterodyne spectroscopy under good weather conditions. Expected upper limits from CSO observations would be about 6×10^{-10} and 2×10^{-9} for HBr and HI, respectively.

6.2. *Mars*

6.2.1. O_2 *and oxygen-bearing molecules.* O_2. Oxygen was detected on Mars, with a mixing ratio of 1.3×10^{-3}, from ground-based high-resolution spectroscopy in the visible range (Carleton and Traub, 1972); this result was later confirmed by the *Viking* mass spectrometer experiment.

As for Venus, oxygen can be observed on Mars in the submillimeter range. The 424 GHz transition, observable with FIRST, is expected to be easily detectable (Fig. 24). Assuming a constant O_2 mixing ratio of 0.0013, a S/N of about 80 should be achieved in 1 h of integration time (case C).

$^{16}O^{18}O$. The $^{16}O^{18}O$ transition at 234 GHz could be searched for at IRAM (Fig. 25). Its detection is likely to require a few hours of integration, but should be feasible, assuming, on the basis of the *Viking* measurements, a solar value of the $^{16}O/^{18}O$ ratio.

O_3. Ozone has been detected on Mars in the UV range, and more recently in the IR (Espenak *et al.*, 1991); it shows strong seasonal, latitudinal and local effects. Its maximum lies at an altitude of about 50 km, with a mixing ratio of about 10^{-6} at the time of maximum abundance. Ozone appears to be maximum in northern winter at high latitude (Krasnopolsky, 1986).

Ozone could be searched for in the millimeter and submillimeter range, at 239 and 610 GHz. At 239 GHz, assuming the "maximum" O_3 distribution, a temperature contrast of 1.5 K is expected (Fig. 26), which would be detectable at IRAM (case A), with a S/N of about 70 in 1 h integration time. However, this calculation implies a uniform "maximum" ozone distribution over the Martian disk, which is too optimistic. Searching for O_3 at 610 GHz

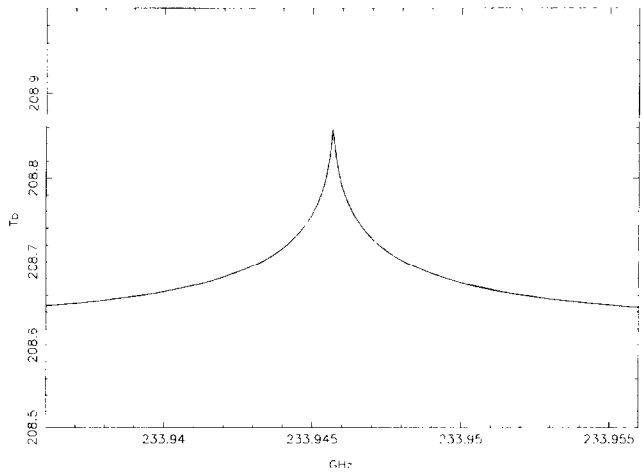

Fig. 25. The synthetic spectrum of $^{16}O^{18}O$ on Mars (234 GHz). The assumed O_2 (constant) mixing ratio is the same as in Fig. 24. The $^{18}O/^{16}O$ ratio is 1/500

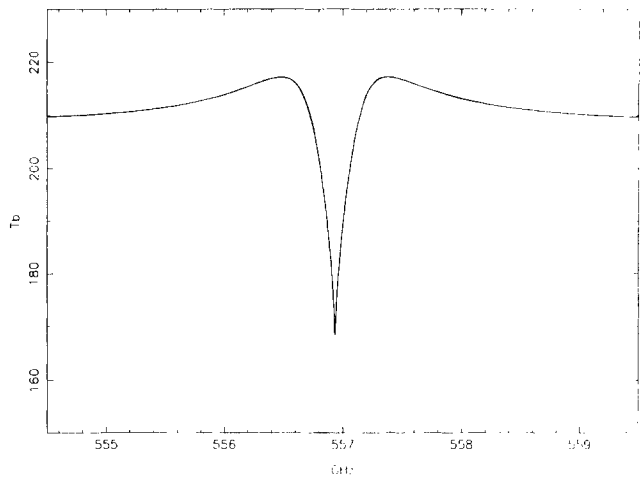

Fig. 27. The synthetic spectrum of H_2O on Mars (557 GHz). The assumed H_2O mixing ratio is 3×10^{-5}. No saturation occurs in this model, so that H_2O/CO_2 is constant with altitude

at CSO will be possible too, as the O_3 line intensity is stronger. The two limits are expected to be comparable.

H_2O. The water vapor on Mars has been detected by several means, using optical and near-infrared spectroscopy from Earth and space. The *Viking* MAWD (Mars Atmospheric Water Detectors) and Lander experiments provided measurements of the water column abundance ranging from 1 pr-μm ("precipitable-micron", corresponding to a mixing ratio of about 15 ppm) to about 70 pr-μm (about 1000 ppm). The H_2O abundance is known to show important local, seasonal and interannual variations (Krasnopolsky, 1986; Rosenqvist *et al.*, 1992), with a mixing ratio in the range 10^{-5}–10^{-4}. In addition, the H_2O vertical distribution is constrained by saturation.

A mapping of the 22 GHz H_2O line has been achieved with the VLA (Very Large Array) by Clancy *et al.* (1992), who derived a mean mixing ratio of 10^{-5}, which corresponds to about 3 pr-μm. A tentative detection of the 183 GHz H_2O line has been obtained at IRAM (Encrenaz *et al.*, 1995b). As in the case of Venus, this observation can only be done under exceptional atmospheric conditions.

The best transition for observing H_2O on Mars is the 557 GHz line, observable from space. As shown in Fig. 27, a temperature contrast of 40 K is expected for a mixing ratio of 3×10^{-5} (with this value, no saturation takes place for the nominal thermal profile). This detection would be very easy for FIRST (S/N of 500 in 1 h of integration time, case C), or any smaller space mission having a comparable instrumentation, such as ODIN.

At higher frequencies, H_2O transitions become stronger and stronger. These lines should be easily detectable with the ISO satellite (case E), using the Fabry–Pérot mode of the long-wavelength spectrograph (LWS). As shown in Fig. 27, which displays the 557 GHz transition over a 5 GHz interval, a loss of about 5 in the line contrast will result from the degraded spectral resolution of LWS (0.03 cm^{-1}). H_2O lines observed with the LWS-FP mode of ISO in the 100–180 μm range—as, for instance, the H_2O transition at 2640 GHz (114 μm)—should thus have a line contrast of 5–10 K and be easily detectable.

HDO. Two transitions of HDO, at 226 and 147 GHz, were tentatively detected on Mars, but their identification remains doubtful (Encrenaz *et al.*, 1991b, 1995b).

The most favorable transition is, as in the case of Venus, the 600 GHz line. Assuming a H_2O mixing ratio of 3×10^{-5} and a D/H ratio equal to 5 times the terrestrial value (Owen *et al.*, 1988), we calculate a line contrast of 40 K (Fig. 28), easily detectable with the CSO in a few minutes of integration time. This observation could be attempted also with a ground-based interferometer (case D).

H_2O_2. H_2O_2 could be the elusive oxidant on Mars, that could also explain the lack of organics on this planet. Nominal mid-latitude photochemical models assuming a water vapor mixing ratio of 150 ppm yield 0.1 ppm of H_2O_2 at the surface of Mars, dropping to about 1 ppb at 30 km (Atreya and Gu, 1994, 1995). During times of large H_2O mixing ratios, H_2O_2 could approach 0.5 ppm at the surface.

Assuming, as nominal values, mixing ratios of 10^{-7}, 10^{-8} and 10^{-10} at altitudes of 0, 15 and 30 km, respectively, the H_2O_2 transition at 606 GHz is expected to show a temperature contrast of 3 K, which should be detectable at the CSO with a S/N of 20 in 1 h of integration time (case B, Fig. 29).

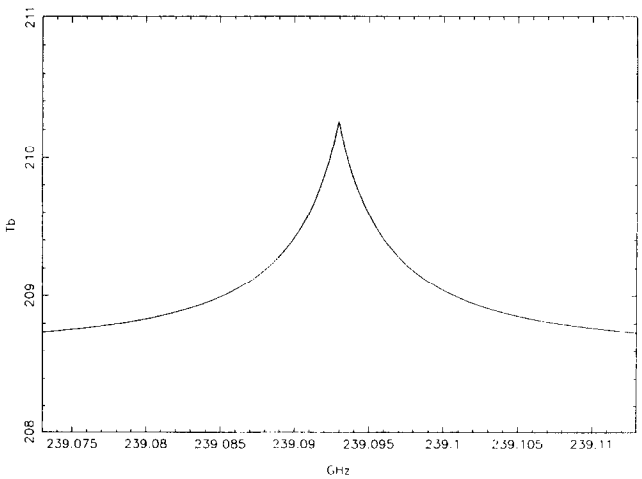

Fig. 26. The synthetic spectrum of O_3 on Mars (239 GHz). The assumed O_3 mixing ratio is 10^{-6} in the 35–60 km range (see text)

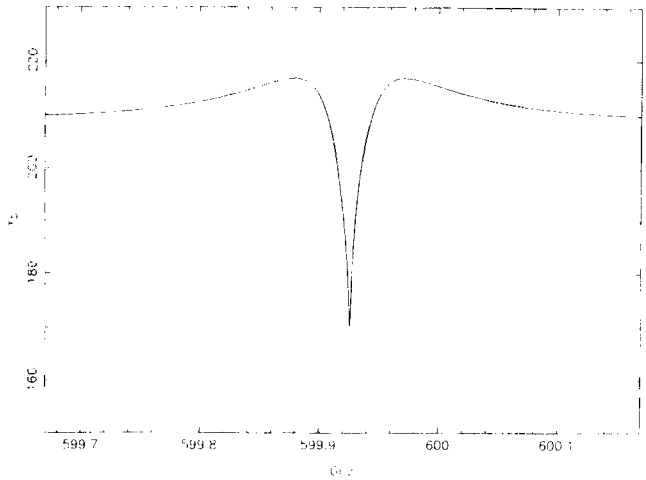

Fig. 28. The synthetic spectrum of HDO on Mars (600 GHz). The assumed H_2O (constant) mixing ratio is the same as in Fig. 27. The D/H ratio on Mars is 6 times the terrestrial value, i.e. 9.0×10^{-4}

At lower frequencies, other transitions, about 10 times lower, are also found. A contrast of 0.3 K should be detectable at IRAM, at 252 GHz (case A), with a S/N of 15 in 1 h of integration time. However, recent unsuccessful attempts (Rosenqvist, priv. commun.) suggest that the actual vertical distribution of H_2O_2 might be less abundant than indicated in the nominal model.

HO_2. This molecule has never been detected on Mars, but photochemical models (Atreya and Gu, 1994) predict a mixing ratio of 10^{-9}. If present at this level, HO_2 could be detectable at CSO in the 600–680 GHz range, in particular at 611 GHz (case B).

6.2.2. *Carbon-bearing molecules.* CO. Like in the case of Venus, CO was the first atmospheric species to be detected on Mars by heterodyne spectroscopy (Kakar *et al.*, 1977). CO and its isotopes have been observed in the ($J = 1$–0), ($J = 2$–1) and ($J = 3$–2) transitions and monitored as a function of time; these observations have provided the CO vertical distribution and the thermal profile. CO has also been mapped over the Martian disk

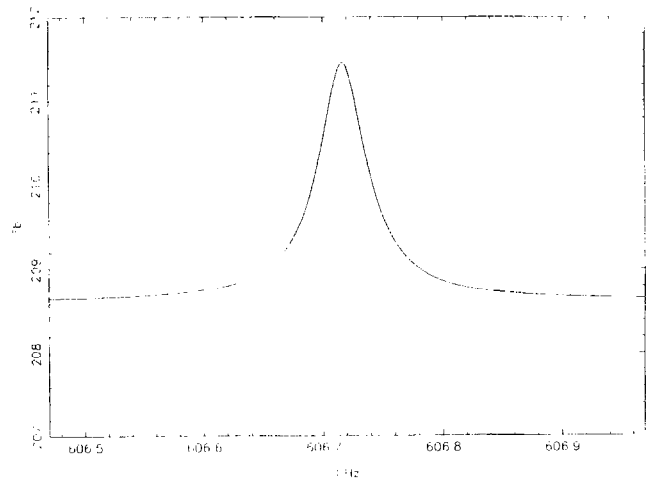

Fig. 29. The synthetic spectrum of H_2O_2 on Mars (607 GHz). The assumed H_2O_2 mixing ratio is 10^{-7} at the surface, 10^{-8} at 15 km (see text)

and wind velocity measurements have been derived (Lellouch *et al.*, 1991a, b).

There is no special need to increase the frequency of these observations, except to improve the spatial resolution for the wind measurements. It should be mentioned that CO transitions corresponding to higher J-values will be observed with the ISO in the LWS-FP mode, with a degraded spectral resolution and no spatial resolution.

H_2CO. A tentative identification of formaldehyde, at 0.5 ppm, has been reported from the Phobos solar occultation data (Korablev *et al.*, 1993). This result was supported by theoretical photochemistry models. However, a subsequent search at 225 GHz, at IRAM, failed to confirm this result (Rosenqvist, priv. commun.).

H_2CO has strong transitions in the submillimeter range. A favorable transition appears at 674 GHz. The corresponding detectability limit at CSO would be a constant mixing ratio of 10^{-10} (case B).

6.2.3. *Sulfur-bearing molecules.* There is presently no positive information about the abundance of gaseous sulfur species on Mars, nor, to our knowledge, any theoretical prediction of their abundances.

SO. From the search of its 220 GHz transition at IRAM, an upper limit of about 10^{-8} can be derived (Lellouch, unpublished result). This upper limit can be improved if a stronger transition is used, like the 688.7 GHz transition at CSO. A constant mixing ratio of about 10^{-10} (1 h integration time) could then be detected (case B).

SO_2. The present upper limit is 3×10^{-8}, from a search of the 216.6 GHz transition at IRAM (Encrenaz *et al.*, 1991b). Using the 689.4 GHz transition at the CSO, one can expect an upper limit of 10^{-9} in 1 h integration.

H_2S. The present upper limit, obtained from the 216.7 GHz H_2S transition at IRAM, is 2×10^{-8} (Encrenaz *et al.*, 1991b). One can expect to reach a detectability limit of 10^{-9} from a 1 h observation of the 611 GHz transition at CSO (case B).

OCS. From the 146 GHz transition, an upper limit of 7×10^{-8} was obtained at IRAM (Encrenaz *et al.*, 1991b). This limit can be reduced to 10^{-9} by using the 243 GHz transition, still at IRAM. There is no real advantage in using lines at higher frequencies.

CS. As in the case of Venus, there is no information about the possible presence of CS on Mars. The detectability limit from the 636 GHz transition would correspond to a constant mixing ratio of 10^{-10}.

6.2.4. *Nitrogen-bearing molecules.* NO. NO was detected in the upper atmosphere of Mars with the *Viking* mass spectrometers (Nier and McElroy, 1977). Its photochemistry has been studied by Yung *et al.* (1977) and McElroy *et al.* (1977). Following their work, we have assumed a NO distribution with a peak of intensity of 5×10^{-6} in the 100–130 km range.

There are two groups of lines which can be considered. The 250 GHz multiplets give a temperature contrast of 0.5 K (Fig. 30), which should be marginally detectable at IRAM with an observation of several hours (case A). The 651 GHz multiplets are expected to give a stronger contrast (1.6 K, Fig. 31), and should be detectable at CSO (case B), with a S/N of 10 in 1 h of integration time.

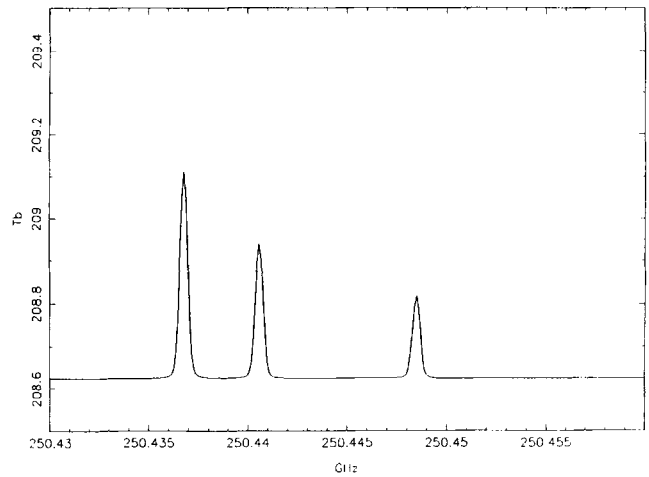

Fig. 30. The synthetic spectrum of NO on Mars (250 GHz). The assumed NO mixing ratio is 5×10^{-6} in the range 100–130 km

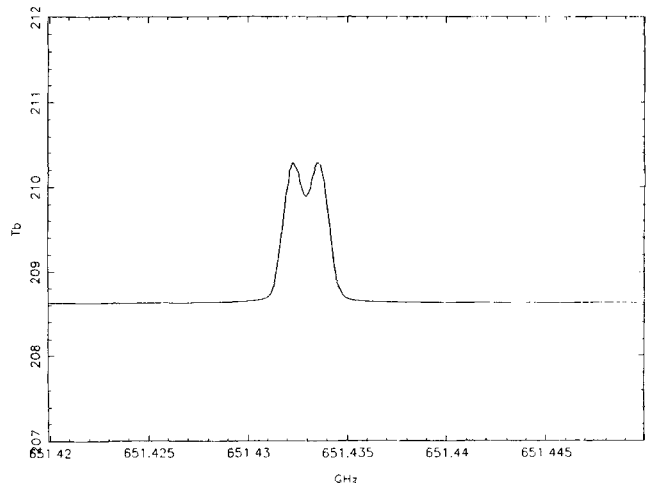

Fig. 31. The synthetic spectrum of NO on Mars (651 GHz). The assumed NO mixing ratio is the same as in Fig. 30

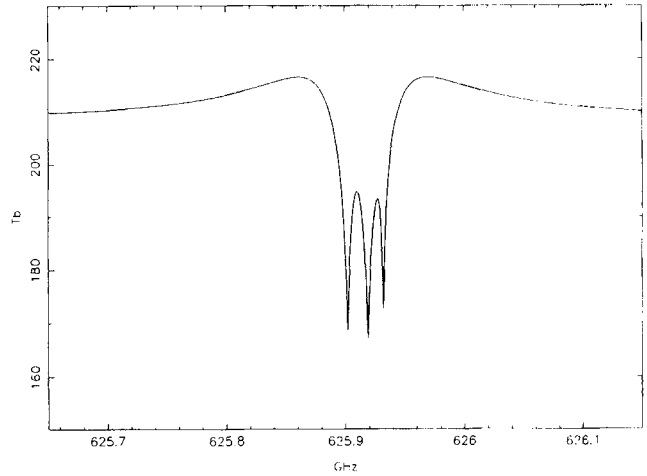

Fig. 32. The synthetic spectrum of $H^{35}Cl$ on Mars (626 GHz). The assumed $H^{35}Cl$ mixing ratio is 4×10^{-7} (constant with altitude)

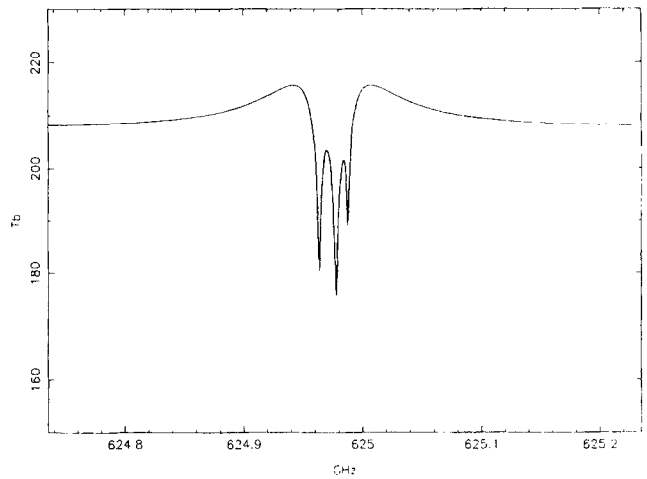

Fig. 33. The synthetic spectrum of $H^{37}Cl$ on Mars (625 GHz). The assumed $H^{35}Cl$ mixing ratio is the same as in Fig. 32. The $^{37}Cl/^{35}Cl$ ratio is 0.325

NO_2 and N_2O. According to Krasnopolsky (1986), the NO_2 mixing ratio on Mars is expected to be 100 times lower than the NO one, and to decrease more rapidly as the altitude increases. There is no information about N_2O, but its formation in measurable amounts is not expected. Taking into account the strengths of the NO_2 and N_2O lines comparable to the NO transitions or weaker, the detection of these species on Mars is thus unexpected.

NH_3. There is no information at present about the possible abundance of ammonia on Mars. A 1 h observation of the 572 GHz line with FIRST should provide a detectability limit of about 10^{-10} (case C).

CN. No information presently exists. As in the case of Venus, an observational limit in the range of 2×10^{-10} is accessible (case A).

6.2.5. HCl, *other* Cl-*bearing molecules and other halides.*

HCl. There is presently no information about the abundance of HCl on Mars. However, if a mixing ratio of 4×10^{-7} is assumed, as in the case of Venus, the two multiplets of HCl and $H^{37}Cl$, at 626 and 625 GHz respectively, should be easily detectable (Figs 32 and 33). As in the case of Venus, the structure of the multiplets should allow a precise retrieval of the HCl vertical distribution. If HCl is less abundant than in Venus, then this observation should provide a detectability limit of about 10^{-10} (case B).

If HCl is present on Mars at the 4×10^{-7} level, the 626 and 625 GHz lines (but not the individual multiplets) should be also observable with a ground-based Fourier-transform spectrometer (case D). In this case, the transitions corresponding to higher J-values should also be easily detectable with ISO (case E).

ClO. There is no information about the possible abundance of ClO on Mars. As in the case of Venus, a search for ClO at 241 GHz using IRAM would provide a detectability limit of about 10^{-8}.

HF and other halides. HF is not detectable in the millimeter or submillimeter range, but has strong transitions in the far-infrared range, which might be observable with ISO. This detection would be easy if the HF abundance on Mars was the same as in Venus. HBr and HI could be detectable too with ISO, and could be searched for with ground-based heterodyne spectroscopy at 500 and 385 GHz, respectively. Expected limits at the CSO (case B) are 6×10^{-10} and 2×10^{-9} for HBr and HI, respectively.

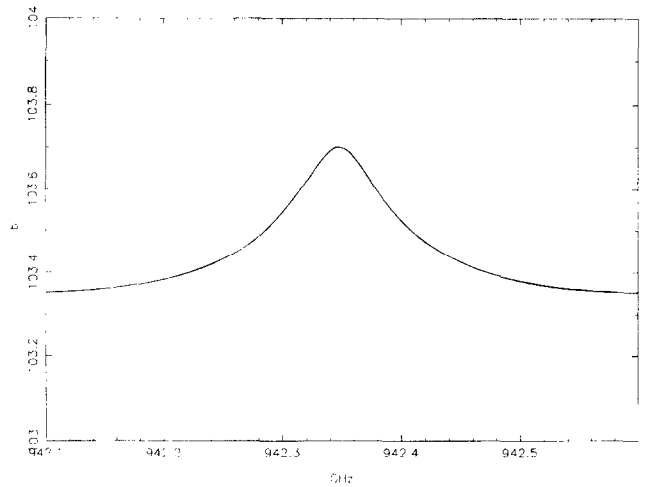

Fig. 34. The synthetic spectrum of CH_4 on Saturn (942 GHz). The assumed CH_4 mixing ratio is 4×10^{-3} (constant with altitude; see text)

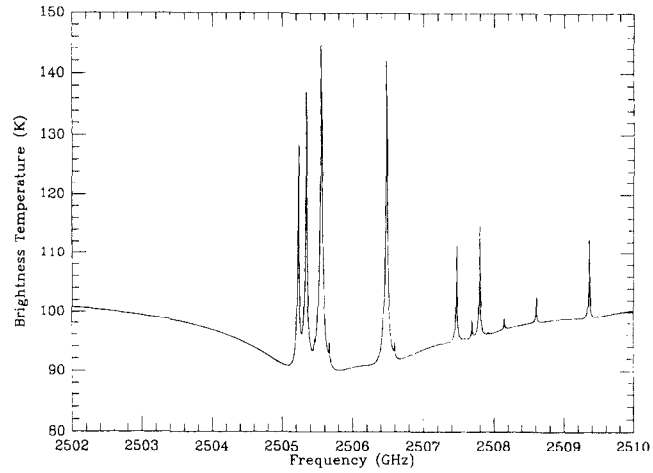

Fig. 35. The synthetic spectrum of CH_4 on Saturn (near 83.6 cm^{-1}, or 2506 GHz). The assumed CH_4 mixing ratio is the same as in Fig. 34

6.3. *Giant planets and Titan*

6.3.1. *Methane and hydrocarbons.* CH_4. Methane is relatively abundant in the atmospheres of the giant planets and Titan: about 2×10^{-3} in Jupiter, 4×10^{-3} in Saturn, in the range of a few 10^{-2} in the tropospheres of Uranus and Neptune, and 2×10^{-2} in Titan's stratosphere (Atreya, 1986). In the case of Uranus and Neptune, saturation is expected to take place in the upper atmosphere, strongly depleting the stratospheric CH_4 mixing ratio; saturation could also take place in Titan's stratosphere. In the other cases, the methane mixing ratio is expected to be constant with altitude up to the microbar level.

CH_4 has been observed through its numerous vibration–rotation bands in the visible and infrared range. However, in the far-infrared and the submillimeter range, it also exhibits weak, forbidden rotational lines, which could be observed in the stratospheres of the giant planets and Titan due to the large atmospheric paths involved. The scientific objectives of such measurements would be the following: determination of the stratospheric thermal profile in the case of Jupiter and Saturn; determination of the stratospheric methane abundance in the case of Uranus, Neptune and Titan.

Transitions corresponding to the lowest J-values can be searched for with heterodyne spectroscopy experiments. As an example, Fig. 34 shows the expected Saturn spectrum of the $J = 4$–3 CH_4 line at 942 GHz, calculated with a methane mixing ratio of 4×10^{-3}. The 0.5 K temperature contrast would be marginally detectable from the ground and/or with FIRST. It should be noted that Saturn, because of its small stratospheric temperature gradient, is not favorable for the detection of stratospheric lines. Jupiter and Neptune are more favorable cases. The CH_4 stratospheric abundance of Neptune, which may correspond to supersaturation, is very uncertain presently. Assuming a stratospheric mixing ratio of 5×10^{-3}, at the upper limit of the uncertainty range (Gautier *et al.*, 1995), a temperature contrast of 2.5 K is obtained. However, because of the large dilution factor, this contrast is not sufficient for the line to be observable from the ground nor from space. In contrast, the CH_4 lines should be observable on Jupiter.

The methane rotational lines are very strong in the far-infrared spectral region, which will be covered by the long-wavelength spectrometer of ISO (case E) as well as FIRST-FP (case F). They should be easily detected on the four giant planets and Titan. In the case of Saturn and Titan, they will also be observed with the CIRS interferometer aboard the *Cassini* orbiter. As an example, Fig. 35 shows the CH_4 multiplet of Saturn at a frequency of 2508 GHz (83.6 cm^{-1}, or 119.6 μm).

CH_3D. The main interest in the CH_3D molecule is that it allows a determination of the D/H ratio, if a simultaneous determination of methane can be obtained in the same atmospheric region (i.e. at a nearby frequency), with the same technique.

CH_3D has been detected in the four giant planets and Titan from its infrared bands. Monodeuterated methane exhibits weak rotational lines near 930 GHz, in the vicinity of the ($J = 4$–3) CH_4 rotational line. The most favorable case is Titan, which shows a deuterium enrichment with respect to Jupiter and Saturn. Assuming a CH_3D mixing ratio of 1.1×10^{-5} (Coustenis *et al.*, 1989), a temperature contrast of 11 K is observed (Fig. 36). This contrast could

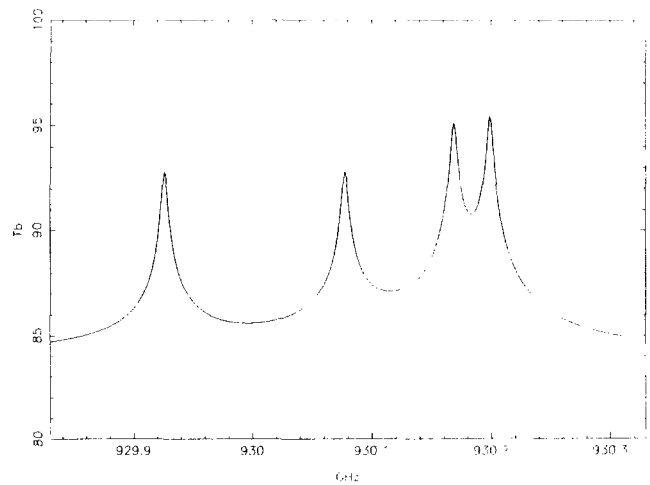

Fig. 36. The synthetic spectrum of CH_3D on Titan (930 GHz). The assumed CH_3D mixing ratio is 1.1×10^{-5} (constant in the stratosphere)

be marginally observable with several hours of integration time (S/N = 0.5 in 1 h). CH_3D is expected to be marginally detectable on Jupiter with the CSO (case B) and with FIRST (case C). It should be noted that heterodyne spectroscopy is definitely needed for this observation, in view of the very narrow line profiles.

C_3H_4. Methylacetylene has been detected in the lower stratosphere of Titan, with an abundance of 4×10^{-9} at the equator and 2×10^{-8} at the north pole (Coustenis *et al.*, 1993). No information exists on the giant planets.

The best frequency to search for C_3H_4 is 257 GHz, where a limit around 10^{-8} could be achieved at IRAM for Jupiter and Saturn, and a value 30 times higher for Neptune and 200 times higher for Titan. In the latter case, this upper limit is thus likely to be meaningless. The Neptune limit is interesting as it is comparable to the value of 2×10^{-7} predicted by Moses *et al.* (1992), while more recent calculations (Dobrojevic *et al.*, priv. commun.) suggest a much lower abundance. Millimeter observations could thus provide a crucial test for these photochemical models.

C_3H_6. Propene (CH_3CHCH_2) has some millimeter transitions, but their intensities are not well known presently. On the basis of present photochemical models, propene is not expected to be present in measurable abundances in the giant planets and Titan.

CH. CH is likely to be a photochemical product of methane, but is not expected to accumulate in the atmospheres of the giant planets. A search for CH at CSO (case B) could lead to a detectability limit in the range of 10^{-10} (Jupiter), 3×10^{-9} (Neptune) and 2×10^{-8} (Titan). Unfortunately, Neptune's expected limit is significantly larger than theoretical estimates from Moses *et al.* (1992) and Dobrojevic *et al.* (priv. commun.), respectively, 10^{-11} and 10^{-13}.

CH_2. CH_2 has several groups of rotational transitions with moderate intensity around 70 GHz, 445 GHz and in the far-infrared range. However, present photochemical models do not predict the formation of CH_2 in any significant amount. A search for CH_2 at IRAM would lead to detectability limits of 4×10^{-10} for Jupiter and Saturn, 10^{-8} on Neptune and 10^{-7} for Titan, probably not significant.

6.3.2. *Nitrogen-bearing molecules.* NH_3. Ammonia is one of the most abundant species in the giant planets. However, its vertical distribution is strongly depleted, both by saturation and by photochemistry, so that its stratospheric abundance is expected to be very low. However, one might not exclude that, in the case of Titan and possibly Neptune, small quantities of stratospheric ammonia might be formed as a product of nitrogen photochemistry.

The first ammonia transition ($J = 1$–0) occurs at 572 GHz, and is not observable from the ground. From heterodyne spectroscopy with FIRST (case C), detectability limits correspond to constant stratospheric mixing ratios ranging from 10^{-10} (Jupiter) to 3×10^{-9} (Neptune) and 2×10^{-8} (Titan). Figures 37 and 38 illustrate the spectra of Neptune and Titan, respectively, calculated with a constant NH_3 mixing ratio of 10^{-10}.

In the case of Jupiter and Saturn, as shown by Lellouch *et al.* (1984a) and Bézard *et al.* (1986), the tropospheric absorption lines of ammonia will be easily detectable with the LWS-FP mode of ISO and the FIRST FP spectrometers.

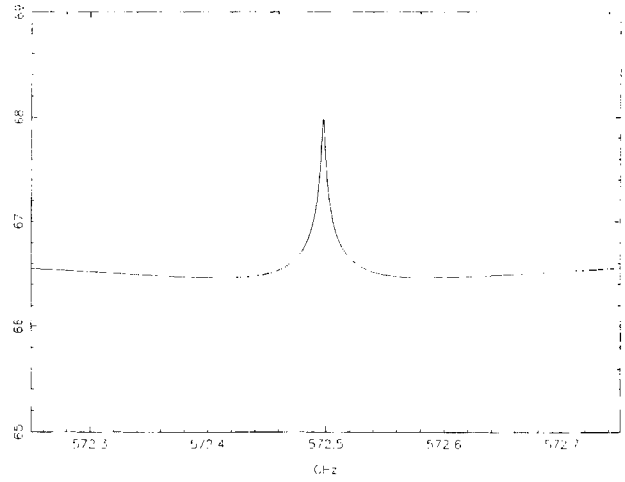

Fig. 37. The synthetic spectrum of NH_3 on Neptune (572 GHz). The assumed NH_3 mixing ratio is 10^{-10} (constant in the stratosphere)

HCN. HCN has been tentatively detected in Jupiter (Tokunaga *et al.*, 1981), using Fabry–Pérot IR spectroscopy. Its origin is likely to be tropospheric. Stratospheric HCN has been detected in the millimeter range on Neptune (Marten *et al.*, 1991, 1993) and Titan (Tanguy *et al.*, 1990), with mixing ratios of 7×10^{-10} and 2×10^{-7}, respectively. The upper limit of stratospheric HCN on Uranus is 7×10^{-10} (Rosenqvist *et al.*, 1992). Recently, HCN has been detected in Jupiter's stratosphere shortly after the impact of comet Shoemaker–Levy-9, and remained observable for a period of several months (Marten *et al.*, 1995).

With its very strong dipole moment, HCN has a series of strong rotational transitions which peak around 1 THz. This is illustrated in Fig. 39 which shows the ($J = 10$–9) HCN spectrum of Neptune at 886 GHz. However, there is no clear advantage of using higher frequency transitions, except for a more accurate retrieval of the vertical stratospheric distribution.

As pointed out by Bézard *et al.* (1986), tropospheric

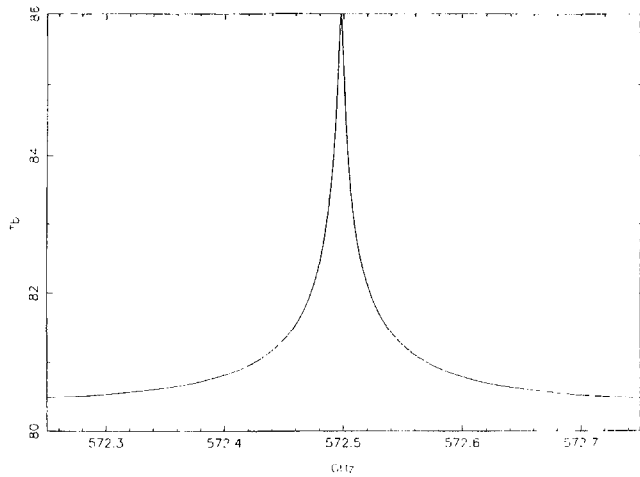

Fig. 38. The synthetic spectrum of NH_3 on Titan (572 GHz). The assumed NH_3 mixing ratio is 10^{-10} (constant in the stratosphere)

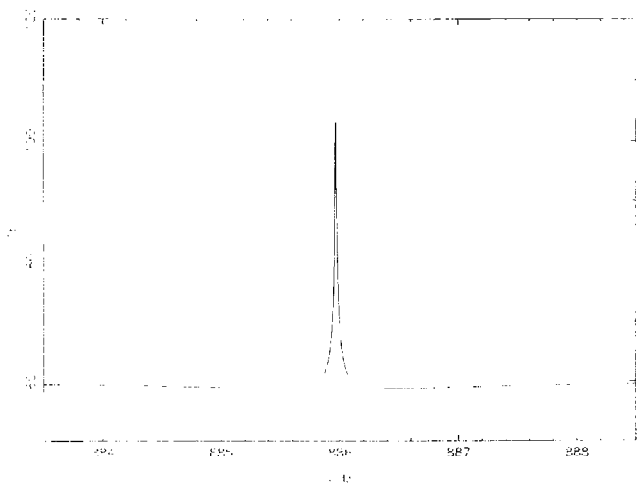

Fig. 39. The synthetic spectrum of HCN on Neptune (886 GHz). The assumed HCN mixing ratio is 7×10^{-10} (constant in the stratosphere)

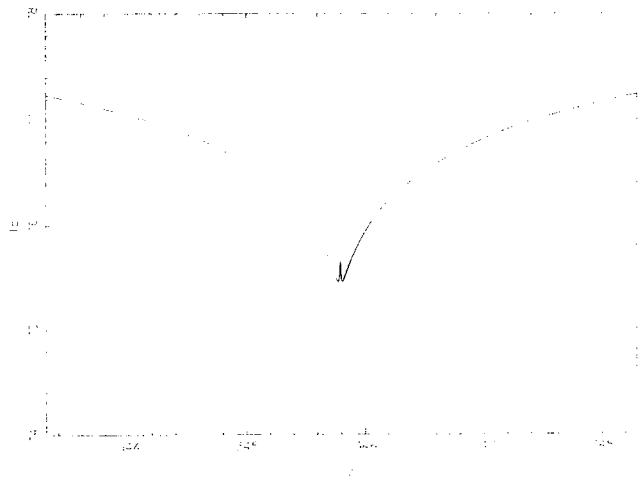

Fig. 40. The synthetic spectrum of CO on Uranus (345 GHz). The assumed CO mixing ratio is 3×10^{-8} (constant with altitude)

lines of HCN are expected to be detectable in the far-infrared spectra of Jupiter and Saturn. They should be easily detectable with the LWS-FP mode of ISO (case E) and the FIRST FP spectrometers (case F). They could also be searched for with a ground-based interferometer (case D). Finally, it should be noted that HCN will be also detectable on Titan in the submillimeter range (Coustenis *et al.*, 1993) with the CIRS interferometer aboard the *Cassini* mission.

CH_3CN. Acetonitrile (CH_3CN) has been recently detected on Titan, at IRAM, with heterodyne spectroscopy at 221 GHz (Bézard *et al.*, 1993a); there is no available information for the giant planets. The detectability limit at 257 GHz, at IRAM, corresponds to a constant stratospheric mixing ratio of 10^{-9} for Jupiter, and 3×10^{-8} on Neptune.

If higher frequency transitions are used, such as the 606 GHz multiplet, a factor of 10 is gained in line intensity, but this advantage is counterbalanced by the smaller size of the CSO antenna and the higher system temperature.

HC_3N. Cyanoacetylene has been detected on Titan, both from IRIS-*Voyager* (see Hunten *et al.* (1984) for a review) and heterodyne spectroscopy (Bézard *et al.*, 1992), at IRAM, at 146 and 218 GHz. The IRIS data led to mixing ratios of 2.5×10^{-7} near 110 km, at high northern latitudes, and an upper limit was derived at intermediate latitudes. The IRAM spectra led to a disk-averaged column density of 10^{14} molec cm^{-2} above the 320 km level. No information exists about its possible abundance in the giant planets.

At 264 GHz, with IRAM, the detectability limit for stratospheric HC_3N is 10^{-10} for Jupiter and 3×10^{-9} for Neptune. Transitions at higher frequencies are not stronger.

CH_2NH. This molecule has never been observed on the giant planets nor on Titan, but appears in some photochemical models as a possible dissociation product. The best spectral range for searching this species is the 230 GHz region, where a detectability limit of 10^{-8} (Jupiter), 3×10^{-7} (Neptune) and 2×10^{-6} (Titan) can be reached with IRAM (case A). There is no definite advantage in using higher frequency transitions.

CN. There is no information about the possible abundance of CN, which is not expected to be stable in the atmospheres of the giant planets and Titan. Upper limits of 10^{-10}, 3×10^{-9} and 2×10^{-8} could be reached with IRAM on Jupiter, Neptune and Titan, respectively.

6.3.3. *Oxygen bearing compounds.* CO. CO has been observed in the tropospheres of Jupiter (Larson *et al.*, 1978) and Saturn (Noll *et al.*, 1986), in the IR range, and in the stratospheres of Neptune (Marten *et al.*, 1991, 1993; Rosenqvist *et al.*, 1992), from heterodyne spectroscopy of the ($J = 2$–1) and ($J = 3$–2) transitions; the ($J = 1$–0) transition was also detected in Neptune's troposphere (Guilloteau *et al.*, 1993). CO was detected in Jupiter's stratosphere following the collision of comet Shoemaker-Levy-9 (Lellouch *et al.*, 1995). In the case of Titan, Lutz *et al.* (1983) first detected CO in the near-infrared and derived a constant mixing ratio of about 10^{-4} in the troposphere. Millimeter heterodyne measurements of CO on Titan (Muhleman *et al.*, 1984) confirmed this value by observing the CO ($J = 1$–0) transition. Later observations of the CO ($J = 1$–0) and ($J = 2$–1) transitions, however, gave a CO mixing ratio about ten times lower in the stratosphere (Marten *et al.*, 1988); this controversy is still not solved. In the case of Uranus, the upper limit for stratospheric CO is 4×10^{-8}. There is little hope of improving this limit, as illustrated by the synthetic ($J = 3$–2) CO spectrum of Uranus (Fig. 40).

Transitions corresponding to $J > 3$ should be detectable in Neptune and Titan, as shown in Figs 41 and 42 which give a comparison of the intensities of the ($J = 3$–2) and ($J = 7$–6) transitions. Such information may be useful for retrieving the CO vertical distribution more accurately. In the case of Jupiter and Saturn, far-infrared absorption lines due to tropospheric CO could be marginally detectable with ISO. Their detection should be easier using either FIRST-FP (case F) or a ground-based interferometer (case D).

H_2O. Tropospheric water is trapped in clouds in the deep atmospheres of the giant planets. However, the presence of stratospheric H_2O has been suggested by various authors in the case of Saturn and Titan. In the case of Saturn this suggestion is based on the possible detection

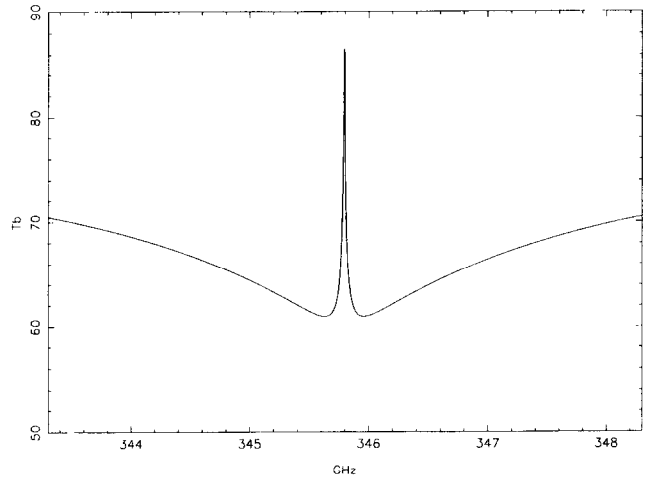

Fig. 41. The synthetic spectrum of CO on Neptune (345 GHz). The assumed CO mixing ratio is 6×10^{-7} (constant with altitude)

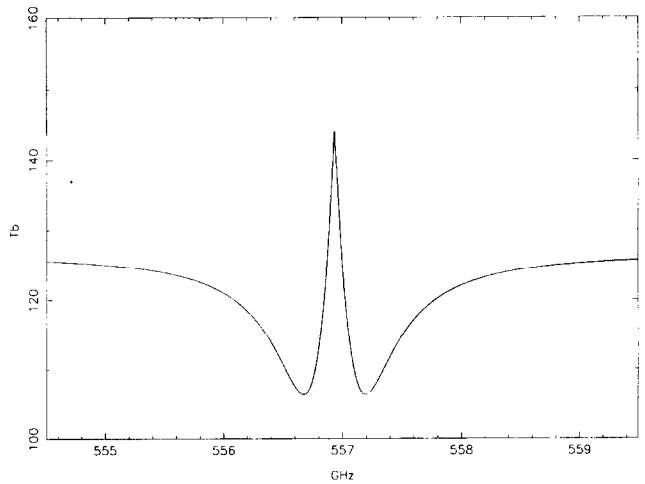

Fig. 43. The synthetic spectrum of H_2O on Saturn (557 GHz). The assumed H_2O mixing ratio is 10^{-7}, constant above the $P = 10$ mbar level (see text)

of H_2O in UV spectra (Wilkenstein *et al.*, 1983); for Titan, the presence of H_2O would be needed to account for the presence of CO_2. In both cases, water would originate from external impacts coming from the rings or from meteorites (Atreya, 1986); measuring the H_2O stratospheric abundance would allow to test the hypothesis of an external flux of particles.

As mentioned above, stratospheric water is best searched for at 557 GHz. Figure 43 shows the synthetic H_2O spectrum of Saturn; our calculations assume a mixing ratio of 10^{-7} above the pressure level $P = 10$ mbar, which corresponds to the column density measured by Wilkenstein *et al.* (1983). It should be mentioned that the transition is very broad. With heterodyne spectroscopy, using a spectral band of 0.5 GHz, a contrast of 30 K is expected; it should be easily detectable with FIRST (case C), and possibly also with a smaller satellite such as ODIN. It should be mentioned that the expected H_2O line is broad enough to be detectable with the LWS-FP mode of ISO (case E), as well as FIRST-FP (case F); with a spectral resolution of 0.03 cm^{-1}, the contrast in the far-infrared H_2O line would be higher than 20 K.

In the case of Titan, assuming, after Coustenis *et al.* (1993), a stratospheric mixing ratio of 10^{-9}, we calculated the 557 GHz H_2O emission line (Fig. 44) which could be also detectable with FIRST in the heterodyne mode (case C). The 35 K contrast would be at the detection limit in 3 h integration time. The detection should be much easier with ISO (case E), using the stronger far-infrared transition lines (Coustenis *et al.*, 1993), or the FP mode of FIRST (case F). For both Saturn and Titan, far-infrared H_2O lines are expected to be observed with CIRS-*Cassini*.

OH. OH, a product of H_2O photodissociation, could be searched for in Saturn and Titan. Rotational transitions are present in the far-infrared range. This detection could be attempted with the LWS-FP mode of ISO (case E).

Other organic molecules: H_2CO, CH_3OH. There is presently no information about the possible abundances of these species in the stratospheres of the giant planets and Titan. We indicate below the expected detectability limits.

In the case of H_2CO, the most suitable range appears in the 600–700 GHz region. In particular, the 674 GHz transition would provide a limit of 10^{-10} for Jupiter and Saturn at the CSO. Because of the dilution factor, this limit is degraded to about 3×10^{-9} for Neptune and

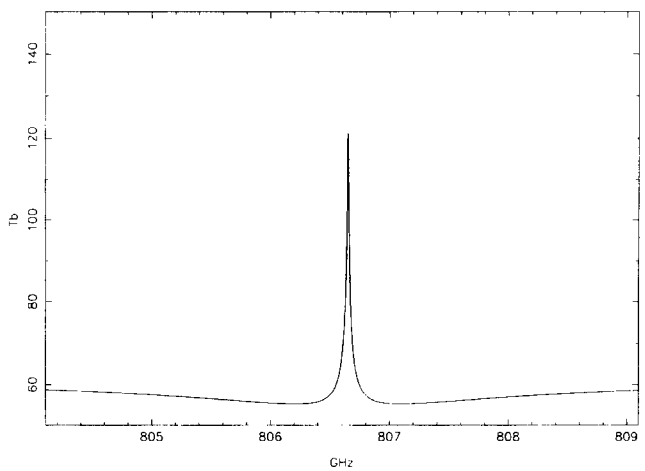

Fig. 42. The synthetic spectrum of CO on Neptune (807 GHz). The assumed CO mixing ratio is the same as in Fig. 41

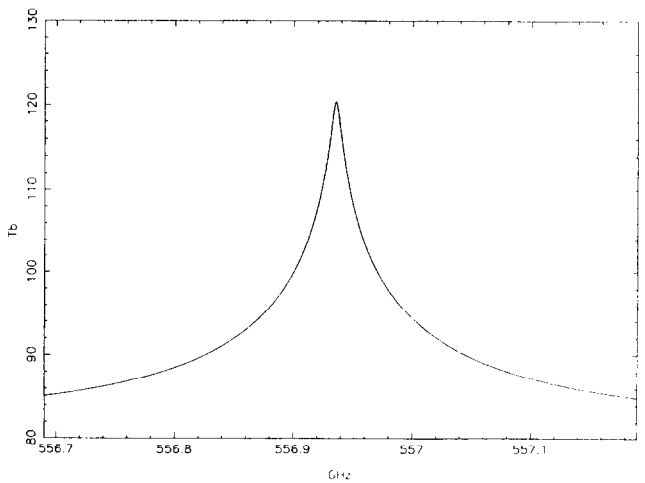

Fig. 44. The synthetic spectrum of H_2O on Titan (557 GHz). The assumed H_2O mixing ratio is 10^{-9}, constant in the stratosphere (see text)

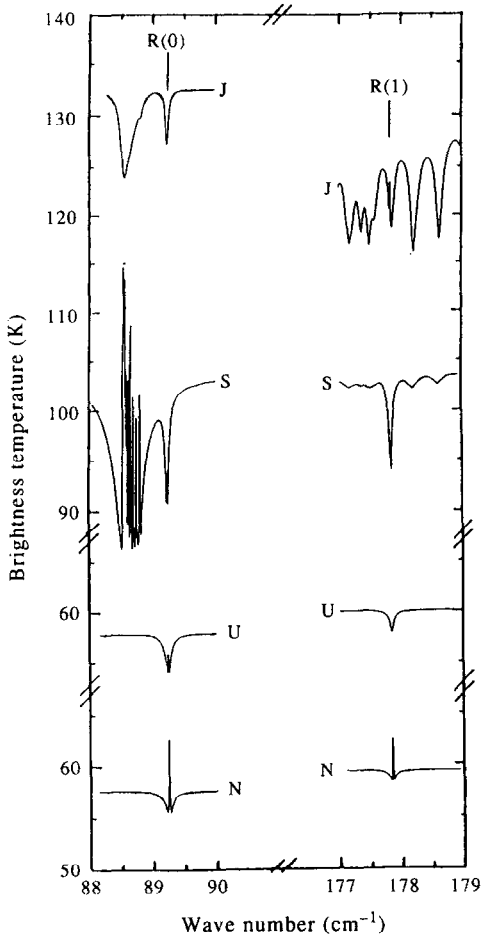

Fig. 45. The synthetic spectrum of HD in the four giant planets (J, S, U and N). The R(0) and R(1) lines are located at 89.23 and 177.84 cm^{-1}, respectively. Other absorption or emission features are due to PH_3 (near the R(0) line) and NH_3 (near the R(1) line). The assumed HD mixing ratio is 6×10^{-5} (constant with altitude). The figure is taken from Bézard *et al.* (1986)

2×10^{-8} for Titan. This latter result is about two orders of magnitude larger than recent theoretical estimates of the H_2CO abundance in Titan's stratosphere (Toublanc *et al.*, 1995).

CH_3OH has a series of transitions around 331 GHz. The corresponding detectability limit with the CSO would be in the range of 10^{-8} for Jupiter and Saturn, about 30 times higher for Neptune and 200 times higher for Titan (case B). Again, the Titan limit is much larger than the present estimate of its abundance (Toublanc *et al.*, 1995).

6.3.4. *Other molecules.* HD. Determining the HD abundance in the giant planets is essential for an accurate measurement of their D/H ratio. Previous determinations rely either on observations of HD lines involving scattering processes in the visible range, difficult to interpret, or on CH_3D analyses, depending upon the fractionation factor. As pointed out by Bézard *et al.* (1986), the best way to derive D/H in the four giant planets is the use of their rotational transitions. The R(0) line, at 89 cm^{-1}, is expected to show up in absorption, with a central core in emission (Fig. 45). Its detection on the four giant planets will be one of the major planetary objectives of the ISO mission.

PH_3. Phosphine has been detected in the tropospheres

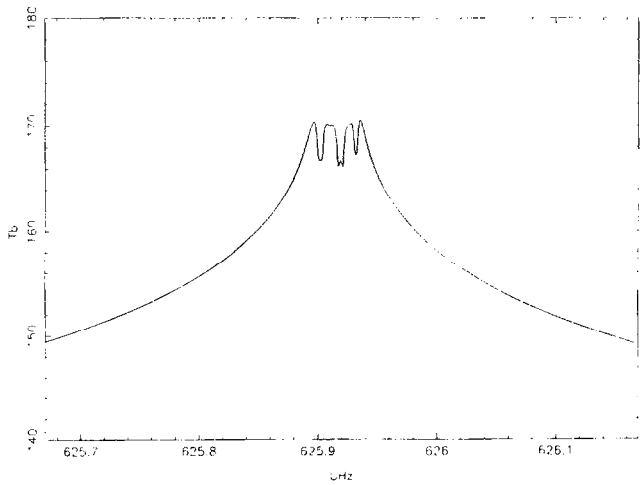

Fig. 46. The synthetic spectrum of $H^{35}Cl$ on Jupiter (626 GHz). The assumed $H^{35}Cl$ mixing ratio is 4×10^{-7} (constant with altitude)

of Jupiter and Saturn from IR spectroscopy. The first rotational line ($J = 1$–0) occurs at 267 GHz. Millimeter heterodyne observations failed to detect an emission core (Lellouch *et al.*, 1984b), which probably implies that, in Jupiter and Saturn, PH_3 is depleted in the upper troposphere by photodissociation. In Uranus and Neptune, PH_3 is likely to condense out in the upper tropospheres of these planets.

The (1–0) PH_3 transition at 267 GHz has been detected in Saturn's troposphere with a ground-based Fourier-transform spectrometer (Weisstein and Serabyn, 1994). The inferred tropospheric mixing ratio is 3×10^{-6}. At 267 GHz, the detectability limit of PH_3 from heterodyne spectroscopy corresponds to a stratospheric mixing ratio of 3×10^{-8} on Jupiter and Saturn.

Tropospheric lines of PH_3 will be easily detectable with ISO (LWS-FP mode, case E) in the case of Jupiter and Saturn. On Uranus and Neptune, the lines are expected to be very marginally detectable. This detection will be easier with a ground-based Fourier-transform spectrometer (case D) or with the FP mode of FIRST (case F).

HCl. No information is presently available on the abundance of HCl in the giant planets. However, Bézard *et al.* (1986) have calculated that, under cosmic abundances (HCl mixing ratio of 4×10^{-7}), and assuming efficient transport from the deep atmosphere where it is stable, HCl rotational lines are expected to be very strong in the far-infrared range.

Assuming a constant mixing ratio of 4×10^{-7} throughout the atmosphere, we have calculated the synthetic spectrum of the 626 GHz $J = 1$–0 transition multiplet, in Jupiter and Saturn (Figs 46 and 47). The strong temperature contrasts would be easily detectable at CSO (case B). The $H^{37}Cl$ isotope would be also observable at 625 GHz; its spectral profile would be comparable to those of $H^{35}Cl$, with slightly lower contrasts.

It should be noted that the assumption of a constant mixing ratio may be unrealistic, as photochemistry is likely to take place at some level in the stratosphere. As in the case of Venus and Mars, the HCl stratospheric

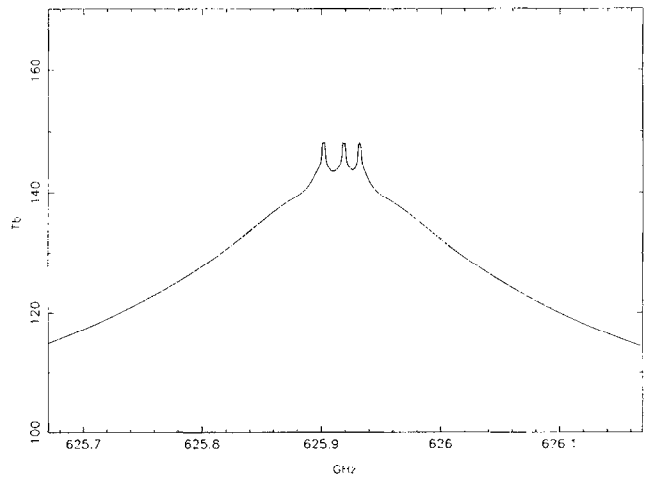

Fig. 47. The synthetic spectrum of $H^{35}Cl$ on Saturn (626 GHz). The assumed $H^{35}Cl$ mixing ratio is 4×10^{-7} (constant with altitude)

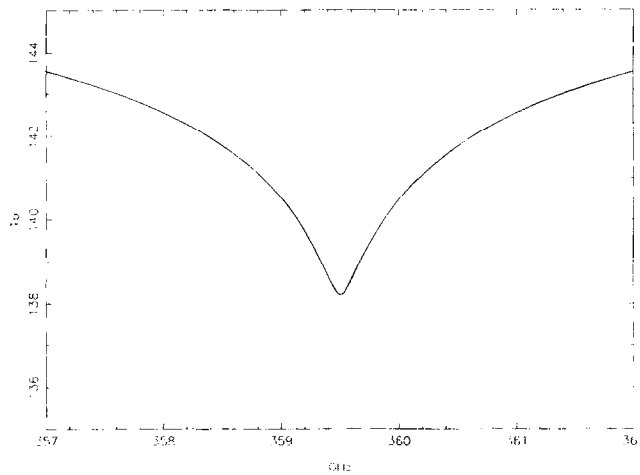

Fig. 48. The synthetic spectrum of HCP on Saturn (359 GHz). The assumed HCP mixing ratio is 10^{-8} (constant with altitude)

vertical profile could be retrieved from the analysis of the HCl multiplet.

As pointed out by Bézard *et al.* (1986), in the case of a constant tropospheric mixing ratio of 4×10^{-7}, the HCl tropospheric lines of Jupiter and Saturn are expected to be easily detectable with the LWS-FP mode of ISO (case E). The same observation could be done with a ground-based Fourier-transform spectrometer (case D) or with FIRST-FP (case F). In the case of Uranus and Neptune, HCl is expected to condense and should not be observable.

In the case of Titan, assuming a cosmic Cl/N abundance ratio, the expected HCl mixing ratio would be 4×10^{-3}. However, HCl is not likely to be stable and might react with Titan's surface. The detectability limit for the 626 GHz line at CSO would be about 10^{-8}.

Other halides: HF, HBr, HI. As for HCl, no information exists presently about the abundances of these species in the giant planets.

Assuming they are present in cosmic abundances (1.5×10^{-7}, 8×10^{-10} and 7×10^{-11} for HF, HBr and HI, respectively), and transported from the deep interior by rapid convective motions, Bézard *et al.* (1986) have shown that all three species are expected to be detectable with ISO (LWS-FP) on Jupiter and Saturn (case E). Emission cores should be observable if their mixing ratio stays constant above the tropopause. As mentioned above (Section 6.1.5), HBr and HI have their first rotational transitions at 500 and 385 GHz, respectively, possibly observable from the ground; but the expected upper limits (6×10^{-10} and 2×10^{-9}, respectively) make their detection difficult (for HBr) or unlikely (for HI).

As in the case of HCl, these species are expected to condense in Uranus and Neptune.

H_2S. On the basis of the cosmic S/H value, hydrogen sulfide would be expected to be relatively abundant in the giant planets (3×10^{-5} in Jupiter's troposphere). Its absence in their IR spectra has been interpreted by chemical reactions involving the formation of NH_4SH clouds in the deep troposphere.

H_2S exhibits a very large number of transitions in the 300–1000 GHz range. Bézard *et al.* (1986) have shown that some of them might be marginally observable in the far IR range. This observation might be made with ISO or, more easily, with a ground-based Fourier-transform spectrometer (case D) or with the FP mode of FIRST (case F).

CS and OCS. Millimeter transitions of CS (J = 5–4, at 245 GHz) and OCS (J = 18–17, at 219 GHz) have been detected at IRAM in the stratosphere of Jupiter, shortly after the collision of comet Shoemaker–Levy-9 (Lellouch *et al.*, 1995). These species are normally absent from Jupiter's stratosphere, but were probably formed as a result of shock chemistry just after the explosion. Their detections in other planets are thus unlikely. In the case of CS, the detectability limit (at IRAM, at 245 GHz) is 2×10^{-11} for Jupiter (under normal conditions) and Saturn, 6×10^{-10} for Neptune and 4×10^{-9} for Titan. These limits are 10 times larger in the case of OCS (at IRAM, at 243 GHz).

HCP. The presence of HCP in Saturn has been suggested on the basis of photochemical models (Kaye and Strobel, 1983), as a photodissociation product of CH_4 and PH_3. Its mixing ratio could be in the order of 10^{-8}. Rotational transitions of HCP occur mostly in the 10–30 cm^{-1} range (Lellouch and Destombes, 1985), and, as calculated by Bézard *et al.* (1986), could be marginally observable in the form of tropospheric absorption lines (Fig. 48). They should be searched for with ISO, FIRST and from the ground (cases D–F).

H_2Se and AsF_3. No information exists about these molecules. Assuming a cosmic abundance of 4×10^{-9} and 4×10^{-10} for H_2Se and AsF_3, respectively, in the tropospheres of Jupiter and Saturn, Bézard *et al.* (1986) have shown that, for the two species, rotational transitions occurring in the 40–90 cm^{-1} range might be observable. As for H_2S and HCP, these observations can be attempted in cases D–F. However, the detection of arsenic in the form of AsH_3 on both Jupiter and Saturn makes the detection of AsF_3 in these planets unlikely.

6.4. *Io, Triton and Pluto*

In the case of these three small bodies surrounded by a tenuous atmosphere, there is still a large uncertainty about

their temperature profile and their chemical composition. We did not calculate synthetic spectra for these objects, but we indicate below possible observations to be attempted, and the corresponding upper limits which might be deduced.

Because the atmospheres of these objects are very tenuous, the lines are Doppler-broadened and extremely narrow. Heterodyne spectroscopy is thus the only means for detecting rotational transitions of gaseous species on these objects.

6.4.1. *Io*. The atmosphere of Io is known to be composed of SO_2, as indicated both by the IRIS infrared data (Pearl *et al.*, 1979) and by the millimeter detection of this molecule at 222 GHz (Lellouch *et al.*, 1990). From the intensity and the width of the observed millimeter line, a surface pressure of 3–40 nbar was inferred, covering only a fraction (5–20%) of Io's surface. The origin of this patchy distribution could be condensation/sublimation processes and/or volcanism. There is a strong uncertainty about the thermal profile: millimeter observations tend to support a hot atmosphere (warmer than 500 K) above the 110 K surface, which aeronomical models presently fail to reproduce. In any case, the temperature contrast between the atmosphere and the surface seems to be a few hundred K, a favorable situation for millimeter observations.

SO_2. After the first detection of SO_2 at 222 GHz at IRAM, several other lines have been searched for (Lellouch *et al.*, 1992). The 143 GHz transition was observed at IRAM, and the 346.6 GHz transition has been tentatively detected at the CSO.

In the future, searching for stronger transitions at higher frequencies, like the 689.4 SO_2 transition, could provide further constraints upon the thermal profile and the SO_2 distributions. This line should be detectable at the CSO.

SO. From the unsuccessful search for SO at 346.5 GHz at the CSO, an upper limit of 5% was derived for the SO mixing ratio, after 8 h of integration (Lellouch *et al.*, 1992). This limit was obtained assuming for SO the same disk distribution as for SO_2, from which its is produced by photodissociation. This upper limit might be improved by the use of the 688.7 GHz transition, which is 4 times stronger.

H_2S. An upper limit of the H_2S abundance was derived from the absence of detection of the 169 GHz line at IRAM. No saturation is expected for this molecule. Assuming a uniform distribution over Io's disk, the corresponding partial pressure is about 0.1 nbar, strongly dependent upon the temperature assumed in the model (Lellouch *et al.*, 1992).

This limit could be improved by using stronger transitions at higher frequencies, for instance the 611 GHz transition, 10 times stronger, at the CSO.

CO. An upper limit of about 5 nbar was reached using the ($J = 1$–0) CO transition at 115 GHz at IRAM; however, this observation was not optimized, as the 1 MHz resolution was used (Lellouch *et al.*, 1992). This limit could be significantly improved by using the 230 GHz line, almost ten times stronger. The ($J = 6$–5) transition at 691 GHz could also be used at CSO. These two lines could provide more stringent upper limits by factors of 10 and 20, respectively.

CS. No information is presently available about the possible abundance of CS; this radical is not expected to be stable on Io. Nevertheless, taking into account the peculiar nature of Io's atmosphere, possibly fed by volcanism, it is still worth mentioning that an upper limit 400 times lower than for CO could be obtained from the 245 GHz transition at IRAM. Another transition, ten times stronger, could be used with the CSO at 685 GHz.

OCS. There is presently no information about the possible abundance of OCS on Io. The best frequency range to search for this molecule is the 230 GHz range. From the 243 GHz transition, a detectability limit of about 0.1 nbar could be expected at IRAM.

6.4.2. *Triton and Pluto*. Our knowledge of the atmospheres of Triton and Pluto has made significant progress over the past years, thanks to three events: the Neptune encounter by *Voyager* 2 in 1989, the Pluto–Charon mutual events in 1985–90 and the observation of a stellar occultation by Pluto in 1988. Both objects have a tenuous, nitrogen-dominated atmosphere, with partial pressures of 10 μbar for Triton and a few μbar for Pluto. In the case of Triton, there is a temperature contrast of about 60 K between the surface and the upper atmosphere (Broadfoot *et al.*, 1989); a similar contrast is also present on Pluto.

Table 3 illustrates that, because of their very large dilution factors, Triton and Pluto fall beyond the detectivity limit of heterodyne spectroscopy. Indeed, whatever the strength of a given transition may be, we cannot expect to observe a brightness temperature contrast larger than the maximum temperature contrast between the upper atmosphere and the surface.

As shown in Table 3, for both Triton and Pluto, the minimum detectable Tb contrasts always exceed 200 K, which rules out any possibility of detecting a molecule on these objects.

7. Conclusions

We present below some concluding remarks about the present and future observational opportunities, as described in our cases A–F.

(A) A 30 m antenna like IRAM remains extremely competitive, as compared to a 10 m antenna working at higher frequency. It should be used preferentially for all molecules having transitions below 300 GHz which are not less than 10 times weaker than those present at higher frequencies. A major improvement would be a 30 m antenna working at 345 GHz under good conditions, i.e. with sensitive receivers and a good antenna efficiency. The advantage of a large antenna is of course decisive for all small objects.

(B) A 10 m antenna like the CSO working in the 300–700 GHz range provides a unique opportunity for molecules like HCl, which present no transitions at lower frequencies. It is also a very good opportunity for molecules having transition intensities which increase significantly with frequency. This is, in particular, the case of SO_2, SO, H_2S, HDO, H_2O_2, O_3.

(C) FIRST, operating in the heterodyne spectroscopy mode, will be unique for molecules like H_2O, O_2 and NH_3,

very important for planetary studies, as well as for all other minor species unobservable from Earth. As shown in Table 3, for extended objects, its excellent system temperature makes this facility as sensitive as a large ground-based antenna.

(D) A ground-based Fourier-transform spectrometer operating in the submillimeter range would be a very precious tool for planetary studies. Due to its moderate spectral resolving power (about 10^4), it would be ideal for detecting tropospheric absorption lines of minor constituents in the atmosphere of Venus or in the tropospheres of the giant planets. In particular, this instrument could be able to detect HCl on all planets, tropospheric HCN and CO on Jupiter and Saturn, and PH_3 in the tropospheres of all giant planets. H_2S, SO and SO_2 lines could also be searched for, especially on Venus. Such an instrument is becoming operational at the CSO (Weisstein and Serabyn, 1994).

(E) The ISO satellite, to be launched by ESA in 1995, will present an excellent opportunity for searching tropospheric species in the giant planets (HD, HCl and other halides), as well as minor constituents on Mars (H_2O), Titan (CO, HCN, H_2O) and possibly Saturn (H_2O). In particular, this facility should be able to provide an accurate determination of the D/H ratio on the four giant planets.

(F) The objectives of FIRST, used in the Fabry–Pérot mode, will be the same as in case E, but they will be easier to achieve, with the increased sensitivity due to the FIRST 3 m telescope. In particular, such an instrumentation will be ideal for searching for weak submillimetric lines in the tropospheres of the giant planets, unobservable from Earth.

In summary, we have seen that many exciting discoveries could be expected in the near future from the exploration of the far-infrared to millimeter spectral range. These new results should significantly enhance our knowledge of the planetary and satellite atmospheres in the forthcoming decade.

Acknowledgements. We wish to thank D. Despois and F. Raulin for their very helpful comments.

References

Anders, E. and Grevesse, N., Abundances of the elements: meteoritic and solar. *Geochim. Cosmochim. Acta* **53,** 197–214, 1989.

Atreya, S. K., *Atmospheres and Ionospheres of the Outer Planets.* Springer, Berlin, 1986.

Atreya, S. K. and Gu, Z., Stability of the Martian atmosphere: is heterogeneous catalysis essential? *J. geophys. Res.* **99,** 13133–13145, 1994.

Atreya, S. K. and Gu, Z., Photochemistry and stability of the atmosphere of Mars. *Adv. Space Res.* 1995 (in press).

Bézard, B., Gautier, D. and Marten, A., Detectability of HD and non-equilibrium species in the upper atmospheres of the giant planets from their submillimeter spectrum. *Astron. Astrophys.* **161,** 387–402, 1986.

Bézard, B., Baluteau, J. P., Marten, A. and Coron, N., The $^{12}C/^{13}C$ and $^{16}O/^{18}O$ ratios in the atmosphere of Venus from high-resolution 10 μm spectroscopy. *Icarus* **72,** 623–634, 1987.

Bézard, B., de Bergh, C., Crisp, D. and Maillard, J. P., The deep atmosphere of Venus revealed by high-resolution nightside spectra. *Nature* **345,** 508–511, 1990.

Bézard, B., Marten, A. and Paubert, G., First ground-based detection of cyano-acetylene on Titan. *BAAS* **24,** 953–954, 1992.

Bézard, B., Marten, A. and Paubert, G., Detection of acetonitrile on Titan. *BAAS* **25,** 1100–1100, 1993a.

Bézard, B., de Bergh, C., Fegley, B., Maillard, J. P., Crisp, D., Owen, T., Pollack, J. B. and Grinspoon, D., High-resolution spectroscopy of sulfur dioxide below the clouds of Venus. *Geophys. Res. Lett.* **20,** 1587–1590, 1993b.

Broadfoot, A. L., Atreya, S. K., Bertaux, J. L., Blamont, J. E., Dessler, A. J., Donahue, T. M., Forrester, W. T., Hall, D. T., Herbert, F., Holberg, J. B., Hunten, D. M., Krasnopolsky, V. A., Linick, S., Lunine, J. I., McConnel, J. C., Moos, H. W., Sandel, B. R., Schneider, N. M., Shemansky, D. E., Smith, G. R., Strobel, D. F. and Yelle, R. V., Ultraviolet spectrometer observations of Neptune and Triton. *Science* **246,** 1459–1466, 1989.

Carleton, N. P. and Traub, W. A., Detection of molecular oxygen on Mars. *Science* **177,** 988–991, 1972.

Cerceau, F., Raulin, F., Courtin, R. and Gautier, D., Infrared spectra of gaseous mononitriles: application to the atmosphere of Titan. *Icarus* **62,** 207–220, 1985.

Clancy, R. T. and Muhleman, D. O., Diurnal CO variations in the Venus mesosphere from CO microwave spectra. *Icarus* **64,** 157–182, 1985.

Clancy, R. T., Grossman, A. W. and Muhleman, D. O., Mapping Mars water vapor with the very large array. *Icarus* **100,** 48–59, 1992.

Connes, P., Connes, J., Benedict, W. S. and Kaplan, L. D., Traces of HCl and HF in the atmosphere of Venus. *Astrophys. J.* **147,** 1230–1237, 1967.

Connes, P., Noxon, J. F., Traub, W. A. and Carleton, N. P., $O_2(^1\Delta)$ emission in the day and night airglow of Venus. *Astrophys. J.* **233,** L29–L32, 1979.

Conrath, B. J., Gautier, D., Hanel, R., Lindal, G. and Marten, A., The helium abundance of Saturn from Voyager measurements. *Astrophys. J.* **282,** 807–815, 1984.

Conrath, B. J., Gautier, D., Hanel, R., Lindal, G. and Marten, A., The helium abundance of Uranus from Voyager measurements. *J. geophys. Res.* **92,** 15003–15010, 1987.

Conrath, B. J., Gautier, D., Lindal, G. F., Samuelson, R. E. and Shaffer, W. A., The helium abundance of Neptune from Voyager measurements. *J. geophys. Res.* **96,** 18907–18919, 1991.

Coustenis, A., Bézard, B. and Gautier, D., Titan's atmosphere from Voyager infrared observations. II. The CH_3D abundance and D/H ratio from the 900–1200 cm^{-1} spectral region. *Icarus* **82,** 67–80, 1989.

Coustenis, A., Encrenaz, T., Bézard, B., Bjoraker, G., Graner, G., Dang-Nhu, M. and Arié, E., Modeling Titan's thermal infrared spectrum for high-resolution space observations. *Icarus* **102,** 240–260, 1993.

Crovisier, J., Constants for molecules of astrophysical interest (available from anonymous ftp at 145.238.2.21/pub/molecule), 1993.

de Bergh, C., Bézard, B., Owen, T., Crisp, D., Maillard, J. P. and Lutz, B. L., Deuterium on Venus: observations from Earth. *Science* **251,** 547–549, 1991.

de Bergh, C., Bézard, B., Crisp, D., Maillard, J. P., Owen, T., Pollack, J. and Grinspoon, D., Water in the deep atmosphere of Venus from high-resolution spectra of the night side. *Adv. Space Res.* **15,** 79–88, 1995.

Encrenaz, T., Remote sensing of the atmospheres of Jupiter, Saturn and Titan. *Rep. Prog. Phys.* **53,** 793–836, 1990.

Encrenaz, T., Lellouch, E., Paubert, G. and Gulkis, S., First

detection of HDO in the atmosphere of Venus at radio-wavelengths: an estimate of the H_2O vertical distribution. *Astron. Astrophys.* **246,** L63, 1991a.

Encrenaz, T., Lellouch, E., Rosenqvist, R., Drossart, P., Combes, M., Billebaud, F., de Pater, I., Gulkis, S., Maillard, J. P. and Paubert, G., The atmospheric composition of Mars: ISM and ground-based observational data. *Ann. Geophys.* **9,** 797, 1991b.

Encrenaz, T., Lellouch, E. and Gulkis, S., Heterodyne spectroscopy of planetary and satellite atmospheres in the millimeter and submillimeter range, in *Coherent Detection Techniques at Millimeter Wavelengths and their Applications* (edited by P. Encrenaz and C. Laurent), pp. 425–453. Nova Science, 1991c.

Encrenaz, T., Lellouch, E., Cernicharo, J., Paubert, G., Gulkis, S. and Spilker, T., The thermal profile and water abundance in the Venus mesosphere from H_2O and HDO measurements. *Icarus* **117,** 162–172, 1995a.

Encrenaz, T., Lellouch, E., Cernicharo, J., Paubert, G. and Gulkis, S., A tentative detection of the 183 GHz water vapor line in the Martian atmosphere: constraints upon the H_2O abundance and vertical distribution. *Icarus* **113,** 110–118, 1995b.

Espenak, F., Mumma, M. J. and Kostiuk, T., Ground-based infrared measurements of the global distribution of ozone in the atmosphere of Mars. *Icarus* **92,** 252–262, 1991.

Gautier, D. and Owen, T., The composition of outer planet atmospheres, in *Origin and Evolution of Planetary and Satellite Atmospheres* (edited by S. K. Atreya, J. B. Pollack and M. S. Matthews), pp. 487–512, 1989.

Gautier, D., Conrath, B. J., Flasar, M., Hanel, R., Kunde, V., Chedin, A. and Scott, N., The helium abundance of Jupiter from Voyager. *J. geophys. Res.* **86,** 8713–8720, 1981.

Gautier, D., Conrath, B. J., Owen, T., de Pater, I. and Atreya, S. K., The troposphere of Neptune, in *Neptune and Triton* (edited by D. Cruikshank and M. S. Matthews). University of Arizona Press, Tucson, 1995 (in press).

Goody, R. M., *Atmospheric Radiation.* Clarendon Press, Oxford, 1964.

Guilloteau, S., Dutrey, A., Marten, A. and Gautier, D., CO in the troposphere of Neptune: detection of the $J = 1$–0 line in absorption. *Astron. Astrophys.* **279,** 661–667, 1993.

Hanel, R. A., Conrath, B. J., Jennings, D. E. and Samuelson, R. E., *Exploration of the Solar System by Infrared Remote Sensing.* Cambridge University Press, London, 1992.

Hunten, D. M., Tomasko, M. G., Flasar, F. M., Samuelson, R. E., Strobel, D. and Stevenson, D. J., Titan, in *Saturn* (edited by T. Gehrels and M. Matthews), pp. 671–759. University of Arizona Press, Tucson, 1984.

Husson, N., Chedin, A., Scott, N., Bailly, D., Graner, G., Lacome, N., Levy, A., Rossetti, C., Tarrago, G., Camy-Peyret, C., Flaud, J. M., Bauer, A., Colmont, J. M., Monnanteuil, N., Hilico, J. C., Pierre, G., Loete, M., Champion, J. P., Rothman, L. S., Brown, L. R., Orton, G., Vanarasi, P., Rinsland, C. P., Smith, M. A. H. and Goldman, A., The GEISA spectroscopic line parameters data bank in 1984. *Ann. Geophys.* **4**(A2), 185–190, 1986.

Janssen, M. A. (ed.), *Atmospheric Remote Sensing by Microwave Radiometry.* Wiley, New York, 1993.

Kakar, R. K., Waters, J. W. and Wilson, W. J., Venus: microwave detection of carbon monoxide. *Science* **191,** 379–380, 1976.

Kakar, R. K., Waters, J. W. and Wilson, W. J., Mars: microwave detection of carbon monoxide. *Science* **196,** 1020–1021, 1977.

Kaye, J. A. and Strobel, D. F., Phosphine photochemistry in Saturn's atmosphere. *Geophys. Res. Lett.* **10,** 957–960, 1983.

Korablev, O. I., Ackerman, M., Krasnopolsky, V. A., Moroz, V. I., Muller, C., Rodin, A. V. and Atreya, S. K., Tentative identification of formaldehyde in the Martian atmosphere. *Planet. Space Sci.* **41,** 441–451, 1993.

Kuiper, G., Identification of the Venus cloud layer. *Commun. Lunar Planet. Lab.* **6,** 100–229, 1968.

Krasnopolsky, V. A., *Photochemistry of the Atmospheres of Mars and Venus.* Springer, Berlin, 1986.

Krasnopolsky, V. A. and Parshev, V. A., Photochemistry of the Venus atmosphere, in *Venus* (edited by D. M. Hunten *et al.*), pp. 431–458. University of Arizona Press, Tucson, 1983.

Larson, H. P., Fink, U. and Treffers, R. R., Evidence for CO in Jupiter's atmosphere from airborne spectroscopic observations at 5 microns. *Astrophys. J.* **219,** 1084–1092, 1978.

Lellouch, E. and Destombes, J. L., Search for minor atmospheric species in the millimeter range of Jupiter and Saturn. *Astron. Astrophys.* **152,** 405–412, 1985.

Lellouch, E., Encrenaz, T. and Combes, M., The detectability of minor atmospheric species in the far infrared spectra of Jupiter and Saturn. *Astron. Astrophys.* **140,** 405–413, 1984a.

Lellouch, E., Combes, F. and Encrenaz, T., Microwave observations of Jupiter and Saturn. *Astron. Astrophys.* **140,** 216–219, 1984b.

Lellouch, E., Gérin, M., Combes, F., Atreya, S. K. and Encrenaz, T., Observation of the $J = 1$–0 CO lines in the Mars atmosphere: radiodetection of ^{13}CO and monitoring of ^{12}CO. *Icarus* **77,** 414–438, 1989.

Lellouch, E., Belton, M., de Pater, I., Gulkis, S. and Encrenaz, T., Io's atmosphere from microwave detection of SO_2. *Nature* **346,** 639–641, 1990.

Lellouch, E., Paubert, G. and Encrenaz, T., Mapping of CO millimeter-wave lines in Mars' atmosphere: the spatial variability of carbon monoxide on Mars. *Planet. Space Sci.* **39,** 219–224, 1991a.

Lellouch, E., Goldstein, J., Bougher, S., Paubert, G. and Rosenqvist, J., First absolute wind measurements in the middle atmosphere of Mars. *Astrophys. J.* **383,** 401–406, 1991b.

Lellouch, E., Belton, M., de Pater, I., Gulkis, S. and Encrenaz, T., The structure stability and global distribution of Io's atmosphere. *Icarus* **98,** 271–295, 1992.

Lellouch, E., Paubert, G., Moreno, R., Festou, M. C., Bézard, B., Bockelée-Morvan, D., Colom, P., Crovisier, J., Encrenaz, T., Gautier, D., Marten, A., Despois, D., Strobel, D. F. and Sievers, A., Chemical and thermal response of Jupiter's atmosphere following the impact of comet Shoemaker–Levy 9. *Nature* **373,** 592–595, 1995.

Lunine, J. I., Atreya, S. K. and Pollack, J. B., Present state and chemical evolution of the atmospheres of Titan, Triton and Pluto, in *Origin and Evolution of Planetary and Satellite Atmosphere* (edited by S. K. Atreya, J. B. Pollack and M. S. Matthews), pp. 605–665. University of Arizona Press, Tucson, 1989.

Lutz, B. L., de Bergh, C. and Owen, T., Titan: discovery of carbon monoxide in its atmosphere. *Science* **220,** 1374–1375, 1983.

McElroy, M. B., Kong, T. Y. and Yung, Y. L., Photochemistry and evolution of Mars' atmosphere: a Viking perspective. *J. geophys. Res.* **82,** 4379–4388, 1977.

Marten, A., Gautier, D., Tanguy, L., Lecacheux, A., Rosolen, C. and Paubert, G., Abundance of carbon monoxide in the stratosphere of Titan from millimeter heterodyne observations. *Icarus* **76,** 558–562, 1988.

Marten, A., Gautier, D., Owen, T., Sanders, T., Tilanus, R., Deane, J. and Matthews, H. E., IAU Circular 5531, August 1991.

Marten, A., Gautier, D., Owen, T., Sanders, T., Matthews, H. E., Atreya, S., Tilanus, R. and Deane, J., First observations of CO and HCN on Neptune and Uranus at millimeter wavelengths and their implications for atmospheric chemistry. *Astrophys. J.* **406,** 285–297, 1993.

Marten, A., Gautier, D., Griffin, M. J., Matthews, H. E., Naylor, D. A., Davis, G. R., Owen, T., Orton, G., Bockelée-Morvan, D., Colom, P., Crovisier, J., Lellouch, E., de Pater, I., Atreya, S., Strobel, D. F., Han, B. and Sanders, D. B., The collision

of comet Shoemaker–Levy 9 with Jupiter: detection and evolution of HCN in the stratosphere of the planet. *Geophys. Res. Lett.* **22,** 1589–1592, 1995.

Moses, J. I., Allen, M. and Yung, Y. L., Hydrocarbon nucleation and aerosol formation in Neptune's atmosphere. *Icarus* **99,** 318–346, 1992.

Muhleman, D. O., Berge, G. L. and Clancy, R. T., Microwave measurements of carbon monoxide on Titan. *Science* **223,** 393–396, 1984.

Na, C. Y., Esposito, L. W. and Skinner, T. E., International Ultraviolet Explorer observation of Venus SO_2 and SO. *J. geophys. Res.* **95,** 7485–7491, 1990.

Nier, A. O. and McElroy, M. B., Composition and structure of Mars' upper atmosphere: results from the neutral mass spectrometers on Viking 1 and 2. *J. geophys. Res.* **82,** 4341–4349, 1977.

Noll, K. S., Knacke, R. F., Geballe, T. R. and Tokunaga, A. T., Detection of carbon monoxide in Saturn. *Astrophys. J.* **309,** L91–L94, 1986.

Owen, T., Maillard, J. P., de Bergh, C. and Lutz, B. L., Deuterium on Mars: the abundance of HDO and the value of D/H. *Science* **240,** 1767–1770, 1988.

Oyama, V. I., Carle, G. C., Whoeller, F., Pollack, J. B., Reynols, R. T. and Craig, R. A., Pioneer Venus gas chromatography of the lower atmosphere of Venus. *J. geophys. Res.* **85,** 7891, 1980.

Paubert, G., Gautier, D. and Courtin, R., The millimeter spectrum of Titan—detectability of HCN, HC_3N and the CO abundance. *Icarus* **60,** 599–612, 1984.

Pearl, J. C., Hanle, R., Kunde, V., Maguire, W., Fox, K., Gupta, S., Ponnamperuma, C. and Raulin, F., Identification of gaseous SO_2 and new upper limits for other gases on Io. *Nature* **288,** 757–758, 1979.

Pickett, H. M., Poynter, R. L. and Cohen, E., Submillimeter, millimeter and microwave spectral line catalog: Revision 3, JPL Technical Publication 80–23, 1992.

Pierce Shah, K., Muhleman, D. O. and Berge, G. L., Measurements of winds in Venus' upper atmosphere based on Doppler shifts of the 2.6 mm ^{12}CO line. *Icarus* **93,** 96–121, 1991.

Pollack, J. B., Dalton, B., Grinspoon, D., Wattson, R., Freedman, R., Crisp, D., Allen, D. A., Bezard, B., de Bergh, C., Giver, L. P., Ma, Q. and Tipping, R., Near-Infrared Light from Venus' nightside: a spectroscopic analysis. *Icarus* **103,** 1–42, 1993.

Poynter, R. L. and Pickett, H. M., Submillimeter, millimeter and microwave line catalog, JPL publication 80–23, 1984.

Prinn, R. G., Venus: composition and structure of the visible clouds. *Science* **182,** 1132–1135, 1973.

Raulin, F., Accaoui, B., Bazaghi, A., Dang-Nhu, M., Coustenis, A. and Gautier, D., Infrared spectra of gaseous organics: application to the atmosphere of Titan. II. Infrared intensities and frequencies of C_4-alkanenitriles and benzene. *Spectrochim. Acta* **46,** 671–683, 1990.

Rosenqvist, J., Lellouch, E., Romani, P., Paubert, G. and Encrenaz, T., Millimeter-wave observations of Saturn, Uranus and Neptune: CO and HCN on Neptune. *Astrophys. J.* **392,** L99–L102, 1992.

Seiff, A., Thermal structure of the atmosphere of Venus, in *Venus* (edited by D. M. Hunten *et al.*), pp. 215–279. University of Arizona Press, Tucson, 1983.

Tanguy, L., Bézard, B., Marten, A., Gautier, D., Gérard, E., Paubert, G. and Lecacheux, A., Stratospheric profile of HCN on Titan from millimeter observations. *Icarus* **85,** 43–57, 1990.

Titov, D. V., Possibility of the formation of an aerosol in a chemical reaction between SO_2 and NH_3 under the conditions of the Venus atmosphere. *Cosmic Res.* **21,** 322–325, 1983.

Tokunaga, A., Beck, S., Geballe, T., Lacy, J. and Serabyn, E., The detection of HCN on Jupiter. *Icarus* **48,** 283–289, 1981.

Toublanc, D., Parisot, J. P., Brillet, J., Gautier, D., Raulin, F. and McKay, C., Photochemical modeling of Titan's atmosphere. *Icarus* **113,** 2–26, 1995.

Townes, C. H. and Schawlow, A. L., *Microwave Spectroscopy.* McGraw-Hill, New York, 1955.

Traub, W. A. and Carleton, N. P., *Exploration of Planetary Atmospheres* (edited by A. Woszcyk and C. Iwaniszewska), p. 223. Reidel, Dordrecht, 1974.

Yung, Y. L., Strobel, D., Kong, T. Y. and McElroy, M. B., Photochemistry of nitrogen in the Martian atmosphere. *Icarus* **30,** 26–41, 1977.

Von Zahn, U., Kumar, S., Niemann, H. and Prinn, R., Composition of the Venus atmosphere, in *Venus* (edited by D. Hunten, L. Colin, T. M. Donahue and V. I. Moroz), pp. 299–430. University of Arizona Press, Tucson, 1983.

Weisstein, E. W. and Serabyn, E., Detection of the 267 GHz $J = 1$–0 rotational transition of PH_3 in Saturn with a new Fourier-Transform spectrometer. *Icarus* **109,** 367–381, 1994.

Wilkenstein, P., Caldwell, J., Kim, S. J., Combes, M., Hunt, G. and Moore, V., A determination of the composition of the Saturnian stratosphere using the IUE. *Icarus* **54,** 309–318, 1983.